SIMULATION OF COAXIAL SILICON NANOWIRE SOLAR CELL

A THESIS SUBMITTED IN PARTIAL FULFILLMENT OF THE REQUIREMENT FOR THE AWARD OF THE DEGREE OF

MASTER OF TECHNOLOGY
IN
NANO SCIENCE AND TECHNOLOGY

SUBMITTED BY
APARAJITA MALLICK
01/NST/2010

UNDER THE SUPERVISION OF
DR. RISHU CHAUJAR

DEPARTMENT OF APPLIED PHYSICS

DELHI TECHNOLOGICAL UNIVERSITY
(FORMERLY DELHI COLLEGE OF ENGINEERING)

CERTIFICATE

This is to certify that Miss Aparajita Mallick has done a 1 year Research cum Project Work on the topic entitled 'SIMULATION OF COAXIAL SILICON NANOWIRE SOLAR CELL' under my supervision. The present research work is being submitted to Department of Applied Physics, Delhi Technological University (Formerly Delhi College of Engineering), towards the partial fulfilment of the requirement for the award of the degree of Master of Technology in Nano Science and Technology. The thesis embodies faithful record of research work carried out by Miss Aparajita Mallick. She has worked under my guidance and that this work has not been submitted, in part of full, for any other degree of Delhi Technological University or any other university.

Dr. Rishu Chaujar

Assistant Professor
Delhi Technological University
(Formerly Delhi College of Engineering)
Bawana Road
Delhi-110042

Date: _____

TABLE OF CONTENTS

ACKNOWLEDGEMENTS

I would like to express my gratitude to Prof. R. K. Sinha, Head of Department, Department of Applied Physics, Delhi Technological University, for his guidance and continuous encouragement throughout my project work.

I offer my profound gratitude to my project guide Dr. Rishu Chaujar, Assistant Professor, Department of Applied Physics, Delhi Technological University, for her constant guidance, help and motivation .Her competent guidance, constant encouragement and critical evaluation helped me develop a new insight into my work.

I gratefully acknowledge their contribution and expertise from time to time. They constantly helped me to resolve the difficulties I faced during the course of my project. Their effort and constant co-operation have been a significant factor in the accomplishment of my project.

LIST OF FIGURES

ABSTRACT

Electronic industry always intends to move towards miniaturisation. Emergence of nanotechnology has led way to research into nanoelectronic system, which might serve as a way to keep up with the Moore's law in future.

The Moore's Law states that the number of transistors that can be placed inexpensively on an integrated circuit doubles approximately every two years.

For such nanoelectronic systems, a better alternative to step down line current to a low value, is to design self powered nanoelectronic systems. This thesis deals with one such idea.

It has been shown that silicon nanowires have the potential to give an improved optical absorption. On this principle, coaxial silicon nanowire solar cell with a p-i-n configuration has been fabricated, where p-type material is crystalline silicon and i-type and n-type material is polysilicon, by the researchers at Harvard University . This cell has been shown to power a nanowire AND logic gate and a pH sensor.

This thesis analyses the performance of the coaxial silicon nanowire solar cell using a semi-classical approach by using simulation tool Silvaco ATLAS version 5.16.3.R. Analysis has also been done on a modified design of solar cell by replacing crystalline silicon with polysilicon in the p-type region. Also the impact of variation of i-layer thickness and electrode material on the performance of the cell has been discussed.

1. Introduction

1.1. Solar cell

1.1.1. Definition

A solar cell (also called photovoltaic cell or photoelectric cell) is a solid state electrical device that converts the energy of light directly into electricity by the photovoltaic effect.

Cells are described as photovoltaic cells when the light source is not necessarily sunlight (lamplight, artificial light, etc.). These are used for detecting light or other electromagnetic radiation near the visible range, for example infrared detectors, or measurement of light intensity.[1]

1.1.2. Working of a solar cell

The basis of all solar cells is the basic p-n junction, or a simple diode. A photovoltaic cell is a diode that utilizes incident electromagnetic radiation to generate an electrical current.

The following processes take place in a general photovoltaic cell:

- Presence of a built–in electric field.
  Built in electric field can be achieved by the following ways:
  - Presence of a p-n junction.
  - Presence of a schottky barrier.
- Photogeneration.
  When a photon collides with a valence electron, imparting energy to the electron. If the electron gains energy equal to or greater than the band gap energy of the material then the electron will be freed from the valence bond. Thus, creating an electron-hole pair. This process is called photogeneration.
- Movement of electron-hole under the influence of built in electric field.
  Under the influence of the electric field the electron and the hole move in the opposite direction.
- If both ends are connected, current flows in the outer circuit.
  If the electron can reach the n-side of the material without recombining, electrical current forms that can power an externally connected circuit

1.1.3. History of Solar cell [2]

1839 – The photovoltaic effect was discovered by Alexandre-Edmond Becquerel, who was a French physicist. This was “the beginning” of

the solar cell technology. Becquerel's experiment was done by illuminating two electrodes with different types of light. The electrodes were coated by light sensitive materials, AgCl or AgBr, and carried out in a black box surrounded by an acid solution. The electricity increased when the light intensity increased.

1873 – The photo conductivity of an element, selenium, was discovered by Willoughby Smith, who was an English electrical engineer.

1876 – Selenium produces electrical current when it is exposed to sun light. William Grylls Adams and Richard Evans Day proved that it is possible to convert solar energy into electricity directly, without any moving parts or heat. The solar cell was very inefficient, and it couldn't be used to run any electrical equipment.

1883 – A description of the first solar cells made from selenium wafer were made by Charles Fritts.

1894 – Charles Fritts constructed what was probably the first true solar cell. He coated a semiconductor material (selenium) with an extremely thin layer of gold. The efficiency were only about 1%, so it couldn't be used as energy supply, but were later used as light sensors.

1904 – A German physicist, Wilhelm Ludwig Franz Hallwachs, discovered that a combination of copper and cuprous oxide was photosensitive.

1905 – Albert Einstein published his paper about the photoelectric effect. There he claimed that light consists of “packets” or quanta of energy, which we now call photons. This energy varies only with its frequency (electromagnetic waves, or the “colour of the light”). This theory was very simple, but revolutionary, and it explained very well the absorption of the photons regarding to the frequency of the light.

1914 – Goldman and Brodsky noted that it existed a barrier layer in photovoltaic devices.

1916 – Robert Andrews Millikan provided experimental proof of the photoelectric effect. He was an American experimental physicist who later won the Nobel Prize for his work on the photoelectric effect and for his measurement of the charge of the electron.

1918 – Jan Czochralski, a Polish chemist, developed a way to grow single-crystal silicon. This increased the efficiency of the silicon-based cells considerably.

1923 – Albert Einstein received the Nobel Prize for his theories explaining the photoelectric effect, which he published 18 years earlier.

1930s – Walter Schottky, Neville Mott and some others developed a theory of metal-semiconductor barrier layers.

1932 – Audobert and Stora discover the photovoltaic effect in cadmium sulfide (CdS).

1950s – Bell Labs produce solar cells for space activities.

1951 – A grown p-n junction enabled the production of a single-crystal cell of germanium.

1953 – Dr. Dan Trivich of Wayne State University makes the first theoretical calculations of the efficiencies of various materials of different band-gap widths based on the spectrum of the sun

1954 – Three researchers, Gerald Pearson, Daryl Chapin and Calvin Fuller, at Bell Laboratories discovered a silicon solar cell, which was the first material to directly convert enough sunlight into electricity to run electrical devices. The efficiency of the silicon solar cell, which Bell Labs produced, were 4%, which later increased to 11%. The cells were made by hand and cost $1000 per watt.

1954 – A cadmium sulphide p-n junction was produced with an efficiency of 6%

1958 – Hoffman Electronics achieved 9% efficient PV cells.

1958 – The first PV-powered satellite, Vanguard I, was launched. The solar panel had an area of 100cm² and delivered an effect of approximately 0.1W. The satellite power system operated for 8 years, and is the world's oldest satellite still in orbit (2007).

1958 – Ted Mandelkorn of U.S. Signal Corps Laboratories fabricates n-on-p (negative layer on positive layer) silicon photovoltaic cells,

1959 – Hoffman Electronics achieved 10% efficient commercially available PV cells and demonstrated the use of a grid contact to significantly reduce series resistance.

1959 – Explorer-6 was launched with a PV array of 9600 cells, each only 1 cm x 2 cm.

1960 – Hoffman Electronics achieved 14% efficient PV cells.

1962 – The Telstar communications satellite, launched by Bell Labs, is initial powered(14W) by solar cells.

1963 – A Japanese electronic manufacturer, Sharp Corporation, produces a viable photovoltaic module of silicon solar cells.

1970 – First highly effective GaAs hetrostructure solar cells are created by Zhores Alferov (a Russian physicist) and his team in the USSR.

1972 – The Institute of Energy Conversion is established at the University of Delaware to perform research and development on thin-film photovoltaic and solar thermal systems, becoming the world's first laboratory dedicated to photovoltaic research and development.

1976 – David Carlson and Christopher Wronski of RCA Laboratories produced the first amorphous silicon photovoltaic cells, which could be less expensive to manufacture than crystalline silicon devices. The efficiency was of 1.1%.

1980 – At the University of Delaware, the first thin-film solar cell exceeds 10% efficiency. It's made of copper sulfide(Cu_2S) and cadmium sulfide(CdS).

1981 – Paul MacCready builds the first solar-powered aircraft, the Solar Challenger, and flies it from France to England across the English Channel. The aircraft had over 16,000 solar cells mounted on its wings, which produced a power of 3kW.

1982 – Hans Tholstrup, an Australian, drives the first solar-powered car, the Quiet Achiever, 4,000km between Sydney and Perth in 20 days. That was 10 days faster than the first gasoline-powered car to do so. The maximum speed was 72 km/h, and the average speed was 24 km/h.

1984 – The IEEE Morris N. Liebmann Memorial Award was presented to Drs. David E. Carlson and Christopher R. Wronski at the 17th Photovoltaic Specialists Conference, "for crucial contributions to the use of amorphous silicon in low-cost, high-performance photovoltaic solar cells."

1985 – The University of South Wales breaks the 20% efficiency barrier for silicon solar cells under one sun conditions.

1989 – Reflective solar concentrators are first used with solar cells.

1991 – Efficient Photoelectrochemical cells (PEC) are developed. Each cell consists of a semiconducting photoanode and a metal cathode immersed in an electrolyte. The Dye-sensitized solar cell (DSC), also called Grätzel cells, is invented. It was a new class of low-class DSC.

1992 – University of South Florida develops a 15.9% efficient thin-film photovoltaic cell made of cadmium telluride, breaking the 15% barrier for the first time for this technology.

1994 – The National Renewable Energy Laboratory develops a solar cell, made from gallium indium phosphide and gallium arsenide, that becomes the first one to exceed 30% conversion efficiency.

1996 – Renewable Energy Corporation(REC), a Norwegian solar energy company established.

1996 – EPFL, the Swiss Federal Institute of Technology in Lausanne, achieves 11% efficiency with the DSCs.

1999 – Spectrolab, Inc. and the National Renewable Energy Laboratory develops a photovoltaic solar cell that converts 32.3 percent of the sunlight that hits it into electricity. The high conversion efficiency was achieved by combining three layers of photovoltaic materials into a single solar cell. The cell performed most efficiently when it received sunlight concentrated to 50 times normal. To use such cells in practical applications, the cell is mounted in a device that uses lenses or mirrors to concentrate sunlight onto the cell. Such "concentrator" systems are mounted on tracking systems that keep them pointed toward the sun.

1999 – The National Renewable Energy Laboratory achieves a new efficiency record for thin-film photovoltaic solar cells. The new measurement is of 18.8 percent efficiency.

2000 – Two new thin-film solar modules, developed by BP Solarex, break previous performance records. The company's 0.5-square-meter module achieves 10.8 % conversion efficiency—the highest in the world for thin-film modules of its kind. And its 0.9-square-meter module achieved 10.6% conversion efficiency and a power output of 91.5 watts — the highest power output for any thin-film module in the world.

2001 – TerraSun LLC developes a method of using holographic films to concentrate sunlight onto a solar cell

2003 – REC Solar started production.

2007 – The university of Delaware achieve a 42.8% efficiency solar cell technology.

1.1.4. Different generations of solar cells[2]

Solar cells are usually divided into three main categories called generations. The first generation contains solar cells that are relatively expensive to produce, and have a low efficiency. The second generation contains types of solar cells that have an even lower efficiency, but are much cheaper to produce, such that the cost per watt is lower than in first generation cells. The term third generation is used about cells that are very efficient. Most technologies in this generation is not yet commercial, but there is a lot of research going on in this area. The goal is to make third generation solar cells cheap to produce.

First Generation Solar Cells:

The first generation includes cells consisting of Silicon or Germanium that are doped with Phosphorus and Boron in a p-n junction. This generation is dominating the commercial market. Silicon cells have a quite high efficiency, but very pure silicon is needed, and due to the energy-requiring process, the price is high compared to the power output.

Second Generation Solar Cells:

Amorphous Silicon Cells

In Amorphous Silicon Cells, hydrogen is introduced to the silicon to make it possible to dope the silicon with boron and phosphorus. The cells are built up in this sequence from bottom to top: metal base contact, n-layer, intrinsic layer, p-layer, transparent contact, glass substrate. These cells experience a drop in efficiency when they are exposed to sunlight, and this effect is created in the intrinsic layer. The effect can be reduced by, instead of one layer, using several thinner layers.

Polycrystalline silicon on low cost substrate

These cells use antireflection layers to capture light waves with wavelengths several times greater than the thickness of the cell itself. This can be done by using a material with a textured surface both in front and back of the cell, rather than a flat surface. This causes the

light to change directions and be reflected, and thus travels a greater distance within the cell then the cell thickness.

Copper Indium diSelenide (CIS) Cells

Copper Indium Diselenide consist of $CuInSe_2$. This material is one of the best light absorber known, and about 99% of the light is absorbed before reaching 1 μm into the material. There have been made homojunctions of CIS, but a heterojunction with cadmium sulfide(CdS) has been found to be more stable and efficient.

Cadmium Telluride Cells

These cells are made from a heterojunction with cadmium sulfide, just like the copper indium diselenide. Cadmium telluride cells also have an ideal bandgap(1.44eV).

Third Generation Solar Cells:

There are several technologies in this generation. One of them is Quantum Dot(QD) Solar Cells. These are built up of a semiconductor(silicon) coated with a very thin layer of quantum dots. Quantum dots is just a fancy name of crystals in the size range typically a few nanometers in diameter. These crystals are mixed into a solution and placed on a piece of silicon which is rotated really fast. The crystals are then spread out due to the centrifugal force. The reason these quantum dots are given so much attention is that normally one photon will excite one electron creating one electron-hole pair. The energy loss is the original energy of the photon minus the energy needed to excite the electron(also called the band gap) However, when a photon hits a quantum dot made of the same material, there may be several electron-hole pairs created, typically 2-3, but 7 has been observed.

Another way to increase the efficiency is to use several layers solar cells with different band gaps in a stack. Each layer will utilise light with different wavelengths, and in this way we can get cells with a higher efficiency.

1.1.5. Solar Cell Characteristic

The characteristics of a solar cell are best illustrated using a current voltage curve (called an *I-V* curve) as in Figure 1.1., the voltage is the horizontal axis and the current is the vertical axis.

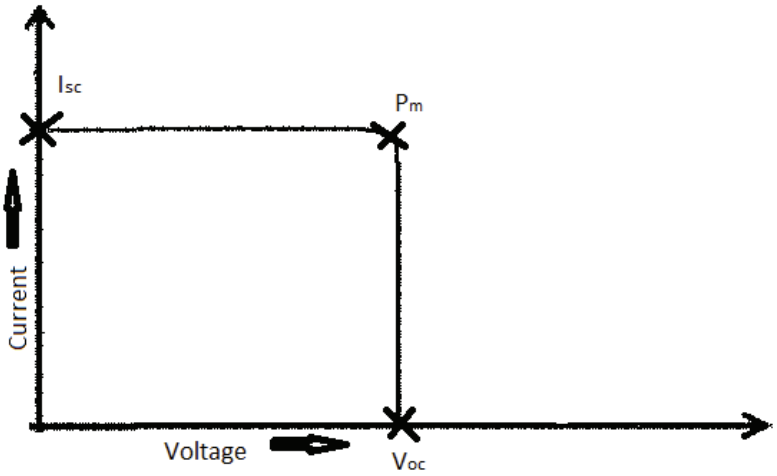

Ideal Characteristic

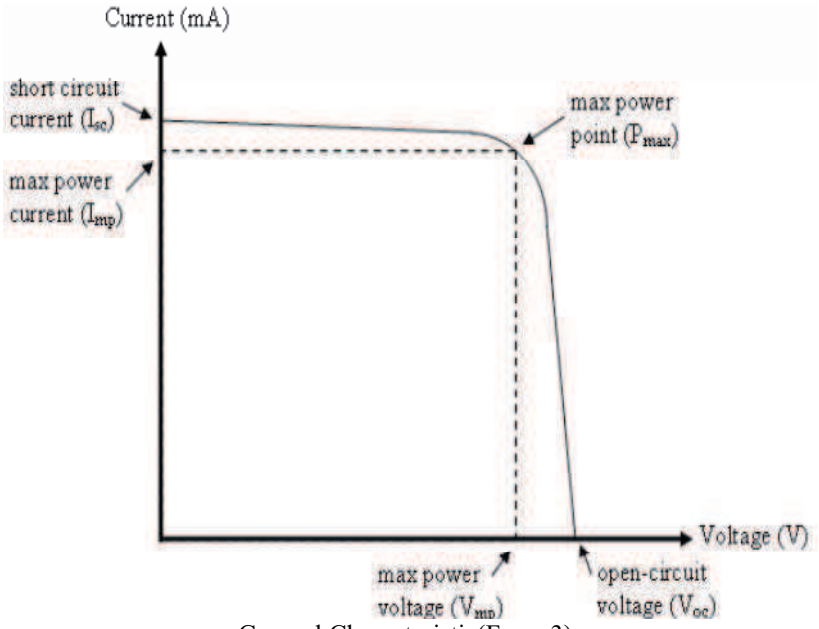

General Characteristic(From 3)

Current-voltage relationship for a simple solar cell.
Figure 1.1.

When the voltage is equal to zero, the cell produces the most current. As the external load is increased, the voltage increases and the current decreases until Voc is reached. At Voc, all excess carriers recombine within the cell and no current is available to power the load.

The parameter maximum power (Pm) point is the point of at which maximum power is produced by the solar cell. Vm and Im are the value of voltage and current respectively corresponding to point of maximum power.

1.1.6. Other Parameters Discussed:

Efficiency of solar cell

Efficiency of a solar cell in percentage is given below:

$$\eta = (P_{in}/P_m) \times 100\%$$

Where Pin is the radiated power striking the cell area from the light source

Fill Factor

Fill Factor (FF) is defined as below::

$$FF = P_m / (I_{sc} \times V_{oc})$$

The fill factor measures the "squareness" of the IV curve.

1.2. Coaxial Silicon Nanowire Solar cell

Solar cells are attractive candidates for clean and renewable power[4],[5]; with miniaturization, they might also serve as integrated power sources for nanoelectronic systems.[6]

Nanoelectronics provide a promising alternative to enhance the performance of electronic devices as well as to continue the scaling of Moore's law[7]. Logic circuits have successfully been fabricated using nanowires [8]. Not only that, researchers from Harvard have shown that self-powered nanosystems are not far beyond our reach [6]. These self-powered nanosystems use solar energy and convert them into electrical power through photovoltaic effect.

In the earlier experiments, nanowires were mostly used simply as a conducting channel for enhancing the electron transport [9], [10]. It was then shown that silicon nanowires have the potential to give an improved optical absorption [11].

1.2.1. Basic Structure:

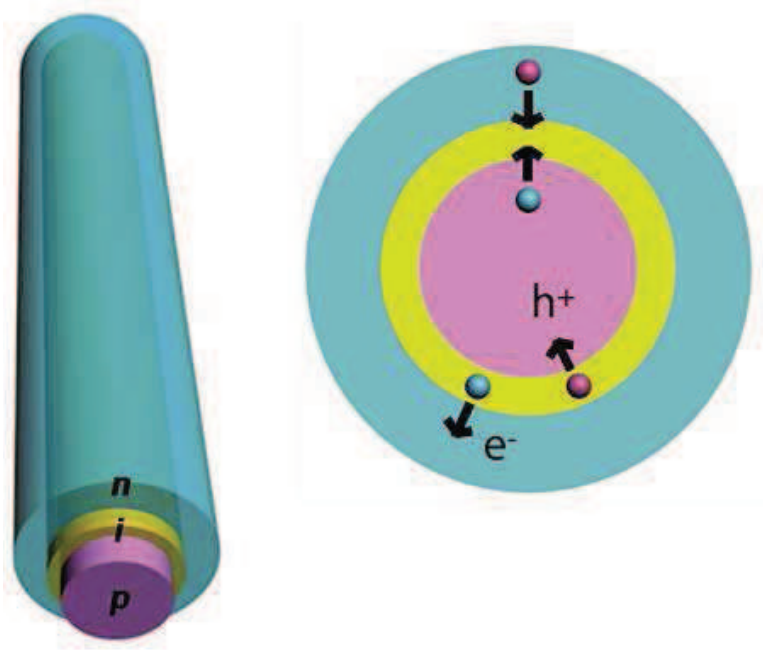

Structure of silicon nanowire solar cell and electron-hole movement (From 6)

Figure 1.2.

The cell consists of a p-i-n coaxial silicon nanowire structures consisting of a p-type silicon nanowire core capped with i- and n-type silicon shells[6]. An advantage of this core/shell architecture is that carrier separation takes place in the radial versus the longer axial direction, with a carrier collection distance smaller or comparable to the minority carrier diffusion length[12]. Hence, photogenerated carriers can reach the p-i-n junction with high efficiency without substantial bulk recombination. An additional consequence of this geometry is that material quality can be lower than in a traditional p-n junction device without causing large bulk recombination[4].

1.2.2. Experimental Background

Fabrication

The coaxial wires were grown in three stages [6]

- The core p-type nanowire is usually synthesized by means of a vapour-liquid-solid (VLS) method.
- This was coated by a chemical vapour deposition with a layer of pure silicon
- The outer n type layer was formed by chemical vapour deposition, during the deposition, phosphine is used as n dopant.
- To get current out of a nanowire solar cell, researchers first etched away its outer two layers at one end. Then they formed metal contacts at both ends.

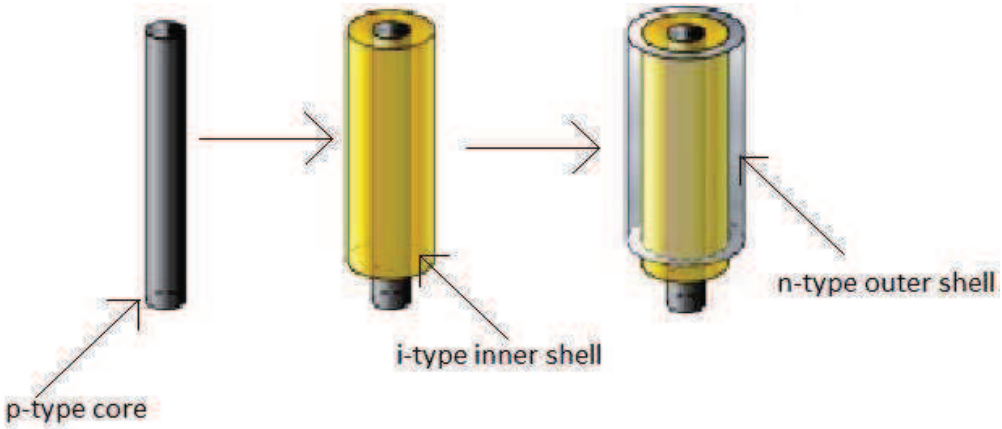

Fabrication of coaxial wire

Figure1.3.

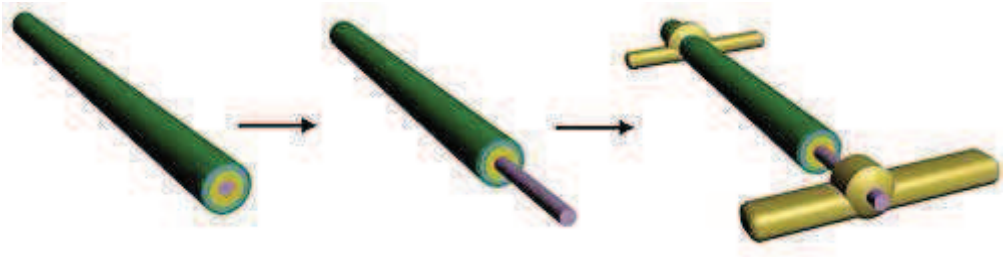

Making Contacts in nanowire solar cell

Figure 1.4

Features[6]:

The fabricated coaxial solar cell has the following features:

- The silicon used is lesser pure as compared the quality usually used for solar cell.
- Due to lesser pure form of silicon, cost is reduced.
- The apparent photovoltaic efficiency of the device is 3.460.2% (upper bound) and 2.360.2% (lower bound).
- Over a year of fabrication and use, the quality of the solar cell has not been degraded.
- It is proposed that the efficiency can be further improved upto 20-25%

Demonstrated application[6]:

- A silicon nanowire pH sensor was powered by a single coaxial silicon nanowire photovoltaic device.
- The operation of AND logic gates fabricated from nanowires and powered by two coaxial silicon nanowires photovoltaic devices.

1.3. Silvaco ATLAS

1.3.1. Introduction to Silvaco ATLAS

This thesis uses Silvaco Atlas version 5.16.3.R to perform solar cell simulation.

ATLAS is a physically-based two and three dimensional device simulator. It predicts the electrical behaviour of specified semiconductor structures and provides insight into the internal physical mechanisms associated with device operation.[13]

The Deckbuilt run-time environment is used in this thesis. The DeckBuilt run-time environment receives the input files. Within the input files, Silvaco Atlas is called to execute the code. Finally, TonyPlot is used to view the output of the simulation Extract statement is used to give run time output.

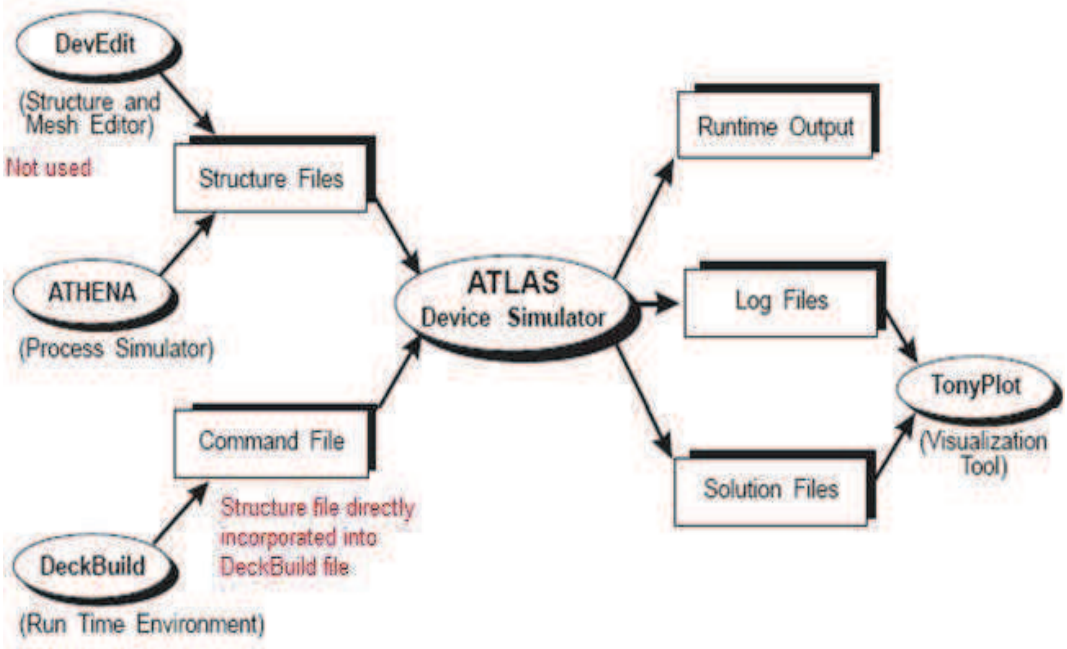

Data Flow in ATLAS (From 13)

Figure 1.5.

1.3.2. Basic program structure of Silvaco ATLAS Program

The order in which statements occur in an ATLAS input file is important. There are five groups of statements that must occur in the correct order. Otherwise, an error message will appear, which may cause incorrect operation or termination of the program.

The order of statements within the mesh definition, structural definition, and solution groups is also important. Otherwise, it may also cause incorrect operation or termination of the program.

Below is written the different groups of statement in the correct order[13]:

Group	**Statements**
1. Structure Specification	MESH REGION ELECTRODE DOPING
2. Material Models Specification	MATERIAL MODELS CONTACT INTERFACE
3. Numerical Method Selection	METHOD
4. Solution Specification	LOG SOLVE LOAD SAVE
5. Results Analysis	EXTRACT TONYPLOT

1.4. AM 1.5 G Spectrum

The efficiency of a solar cell is sensitive to variations in both the power and the spectrum of the incident light. To facilitate an accurate comparison between solar cells measured at different times and locations, a standard spectrum and power density has been defined for both radiation outside the Earth's atmosphere(AM0) and at the Earth's surface.

The standard spectrum at the Earth's surface is called AM1.5G, (the G stands for global and includes both direct and diffuse radiation) or AM1.5D (which includes direct radiation only).

The global spectrum is 10% higher than the direct spectrum. The standard AM1.5G spectrum has been normalized to give 1kW/m^2 due to the convenience of the round number and the fact that there are inherently variations in incident solar radiation.

This thesis uses AM 1.5G for analysis.

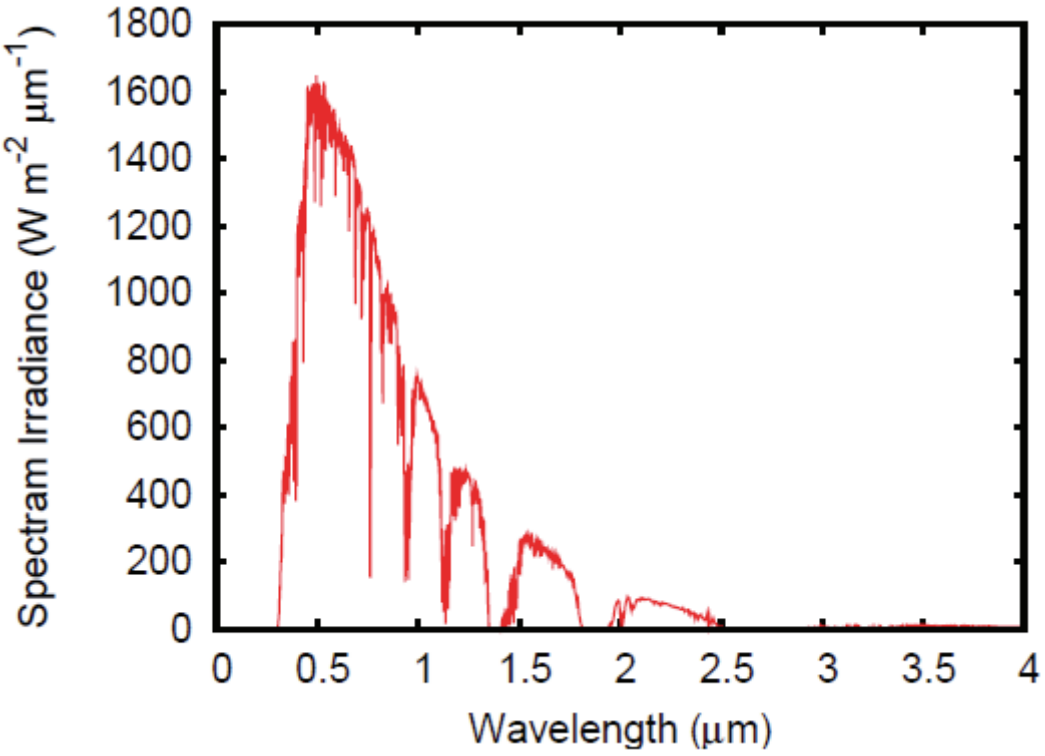

Solar spectrum air mass 1.5 global (AM 1.5 G)

Figure 1.6.

2.Simulation

2.1. Basic simulation details of solar cell

The basic structure of the solar cell consists of a p-type cylindrical core surrounded by an i-type coaxial shell which further is surrounded by a n-type coaxial shell.

p-i-n configuration of silicon nanowire solar cell

Figure 2.1.

- Simulation tool, SILVACO Atlas version 5.16.3.R, is used.
- Due to the radial symmetry of the structure, simulation is done in 2D.
- Cylindrical co-ordinates are used.
- Simulation is done considering Temperature=300K.
- Radius of the p-type core= 50 nm.
- Thickness of the i-layer = 30nm
- Thickness of n layer = 100 nm
- Total diameter = 360 nm.
- Length of the nanowire= Two micron.
- Models used in simulation:
    - Drift Diffusion Model- The transport properties are calculated using the drift diffusion model. The validity of using such a semi-classical approach for the nanowire size considered in this work has been discussed in [11], [12].
    - CONMOB-Concentration dependent mobility[13].
    - CONSRH-Concentration Dependent Shockley-Read-Hall recombination[13].
    - CVT-Transverse field dependent mobility[13].
    - FLDMOB-Lateral Field Dependent Mobility[13].
    - BGN-Band Gap Narrowing[13].
    - OPTR-Optical Recombination[13].
- The doping concentration of p-type region- $1X10^{18}$ cm^{-3}.
- The doping concentration of i-type region - $1X10^{14}$ cm^{-3}.
- The doping concentration of n-type region - $1X10^{18}$ $cm^{-3.}$
- For illumination of the solar cell AM1.5G spectrum is used.

2.2. Device 1

P-type inner cylinder is of crystalline silicon, whereas the i-type and n-type layers are of Polysilicon. This is the structure which discussed in paper [6].

Electrodes selected:

Anode: Gold, 5.3eV Cathode: Molybdenum, 4.53eV

2.2.1. Structure:

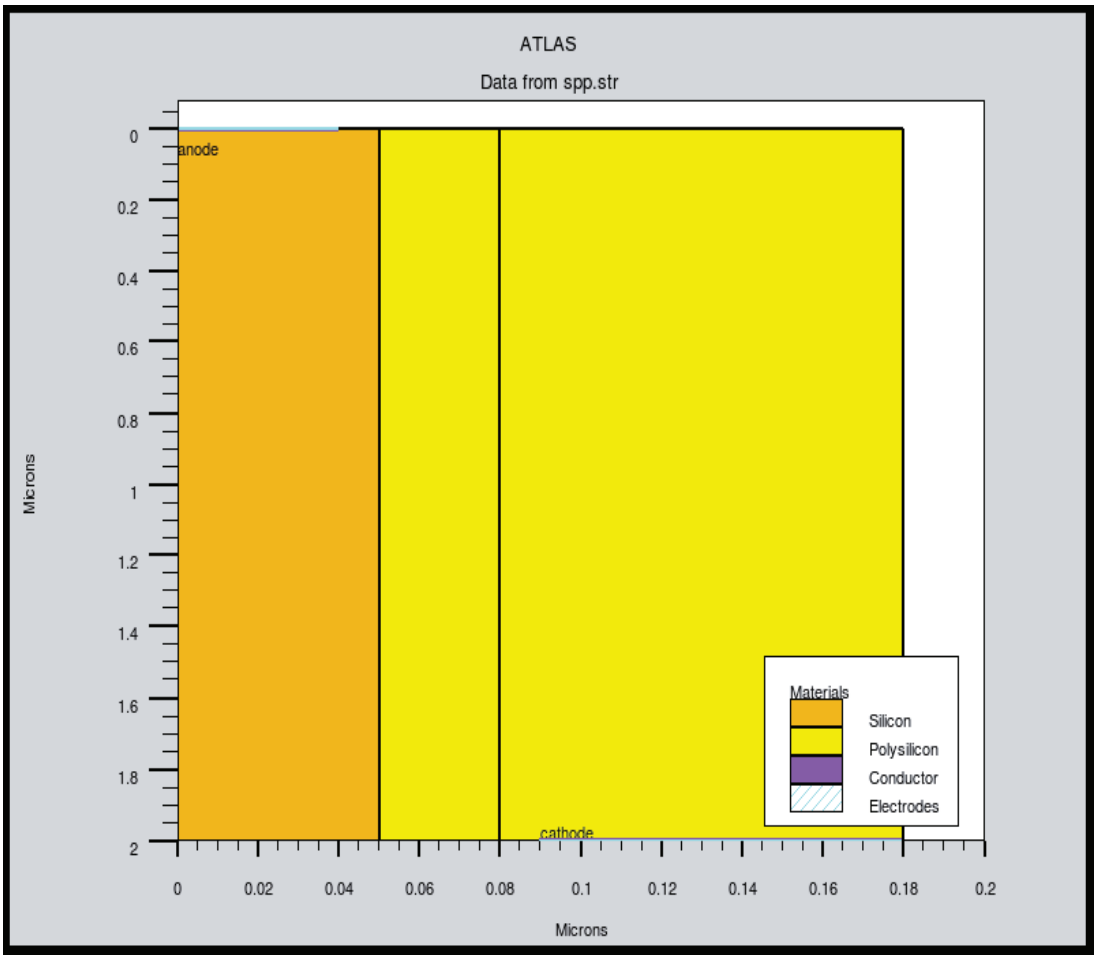

2D simulated structure of Device1

Figure 2.2.

2.2.2. I-V Characteristic

Dark-Current Characteristic:

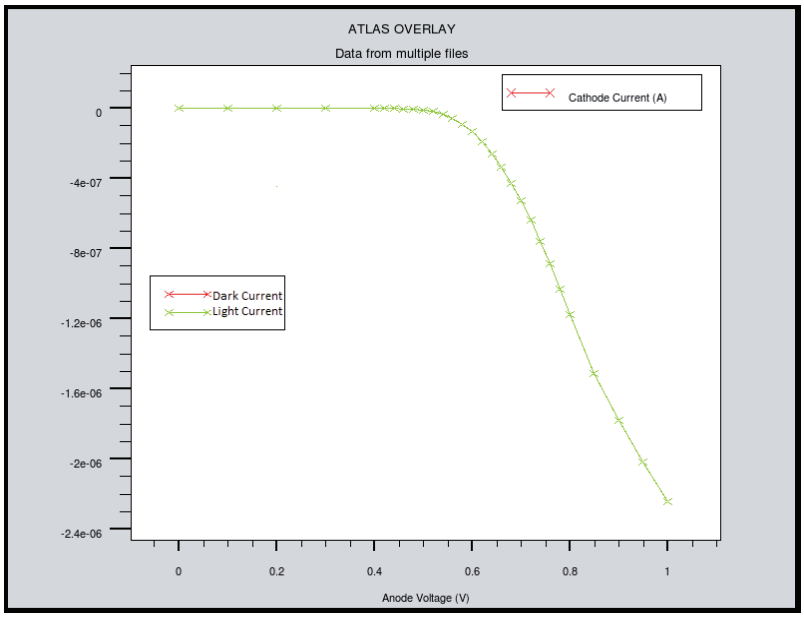

Dark current and light current of Device1

Figure 2.3.

Light-Current Characteristic:

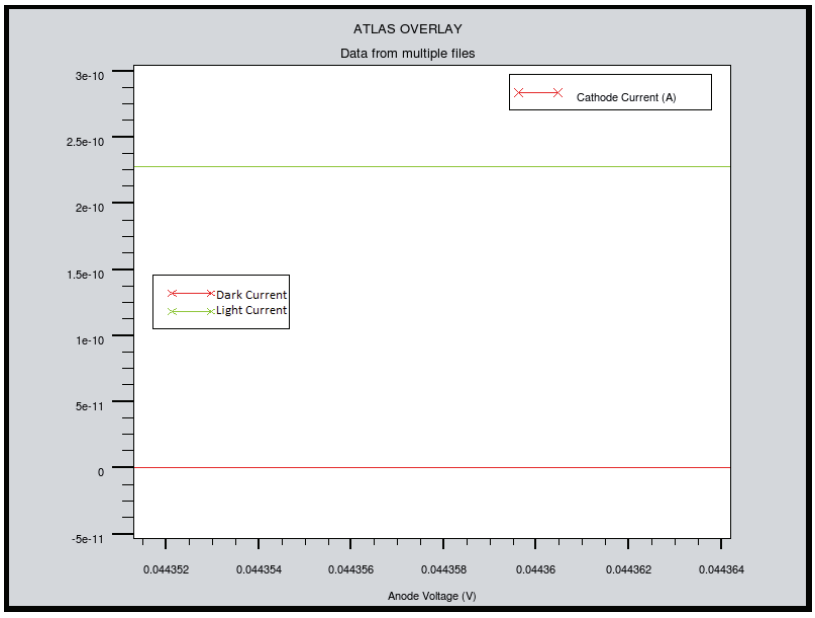

Zoomed view of dark current and light current of Device1

Figure 2.4.

2.2.3. Observation:

Short Circuit Current, Isc:	2.28424×10^{-10} A
Efficiency, Eff:	2.81652%

Comment:

It is observed that the short circuit current, Isc=2.28424×10^{-10} A which is about the same as reported for a nanowire of 2 micron in [6]. As shown in the graph below, taken from the paper mentioned.

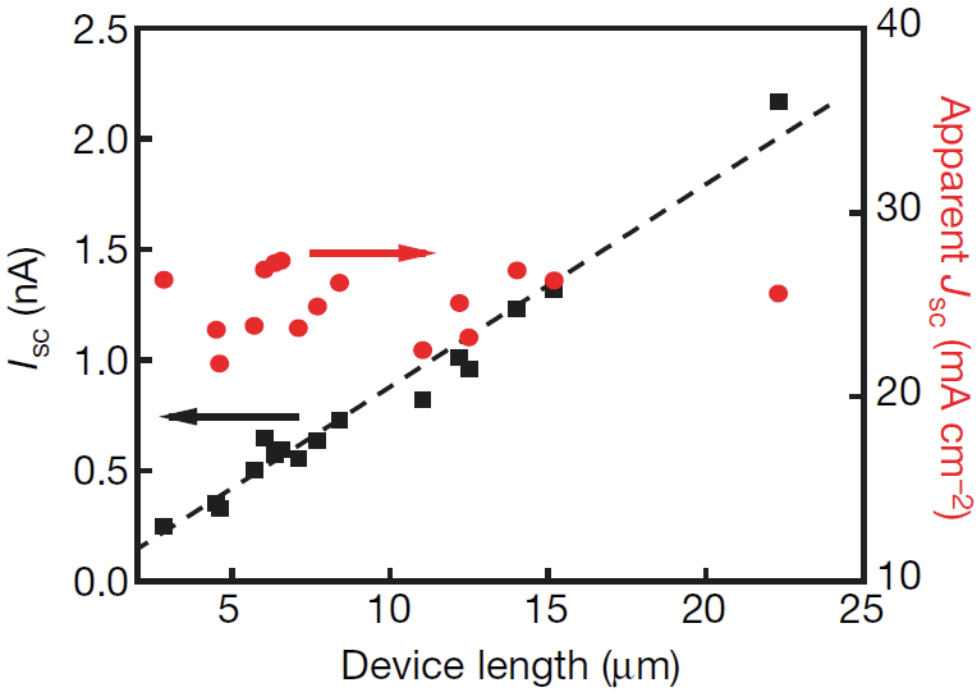

Impact of variation of nanowire length on Isc and Jsc(From 6)

Figure 2.5.

The efficiency is calculated to be 2.81652%, which lies between the experimental range of 2.36±0.2%(lower bound) and 3.46±0.2% (upper bound) as reported in the paper mentioned.

2.3. Device 2

P-type inner cylinder, the i-type and n-type layers are of Polysilicon.

Anode: Gold, 5.3eV Cathode: Molybdenum, 4.53eV

2.3.1. Structure:

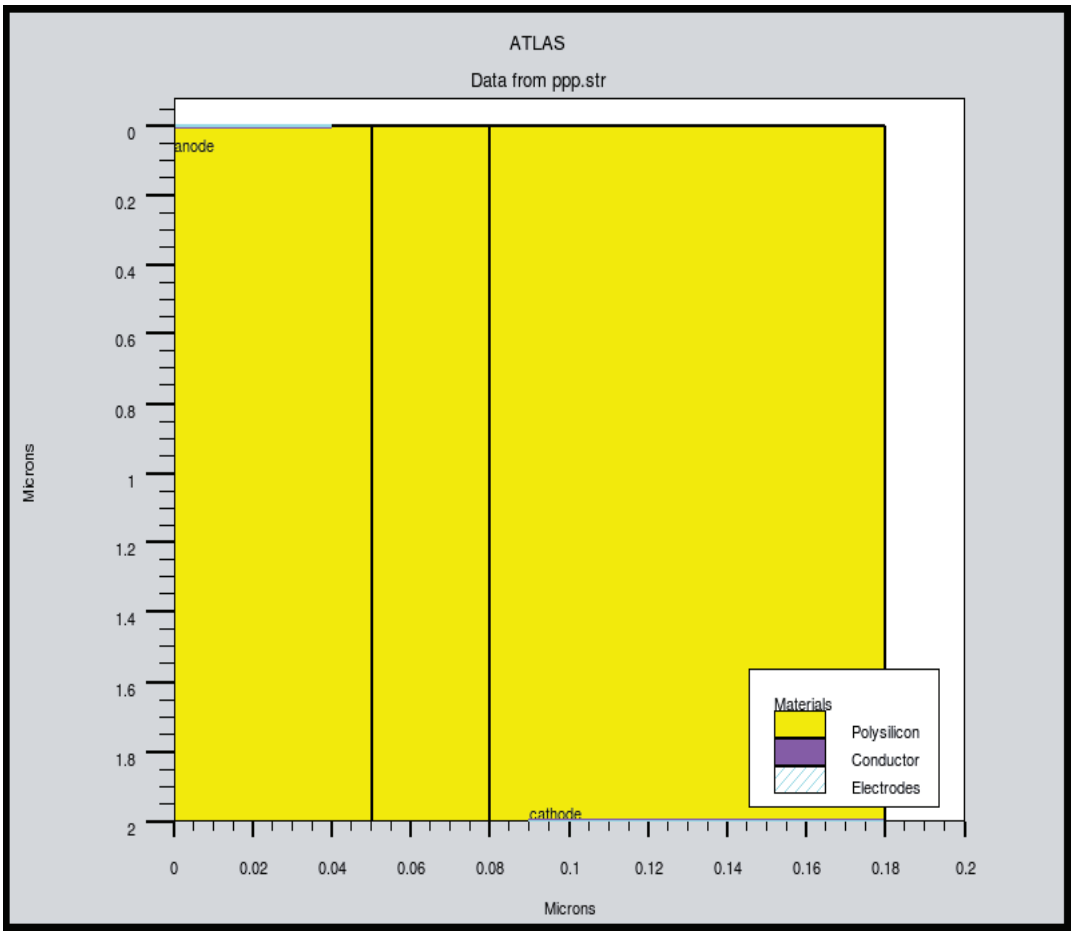

2D simulated structure of Device2

Figure 2.6.

2.3.2. I-V Characteristic

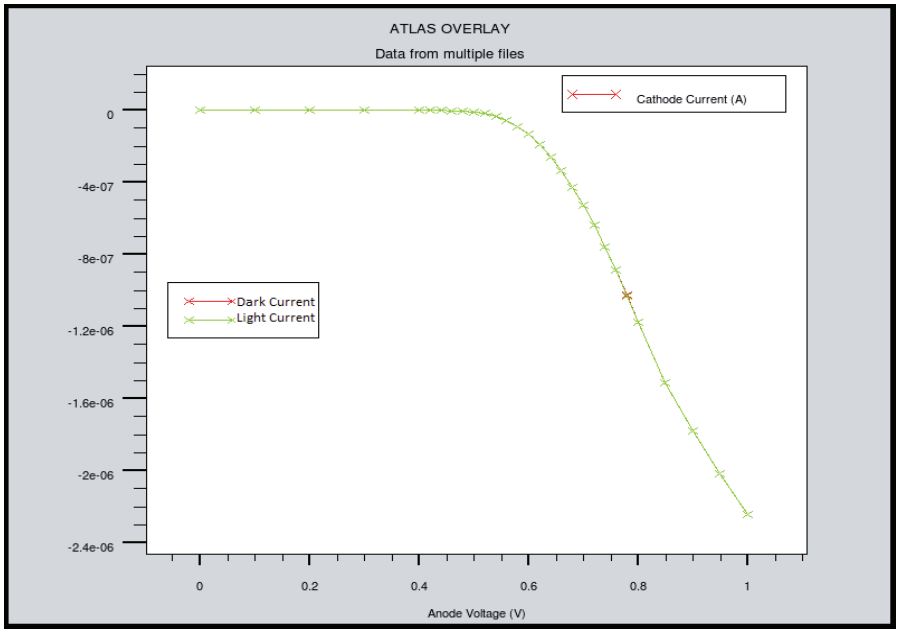

Dark current and light current of Device2

Figure 2.7.

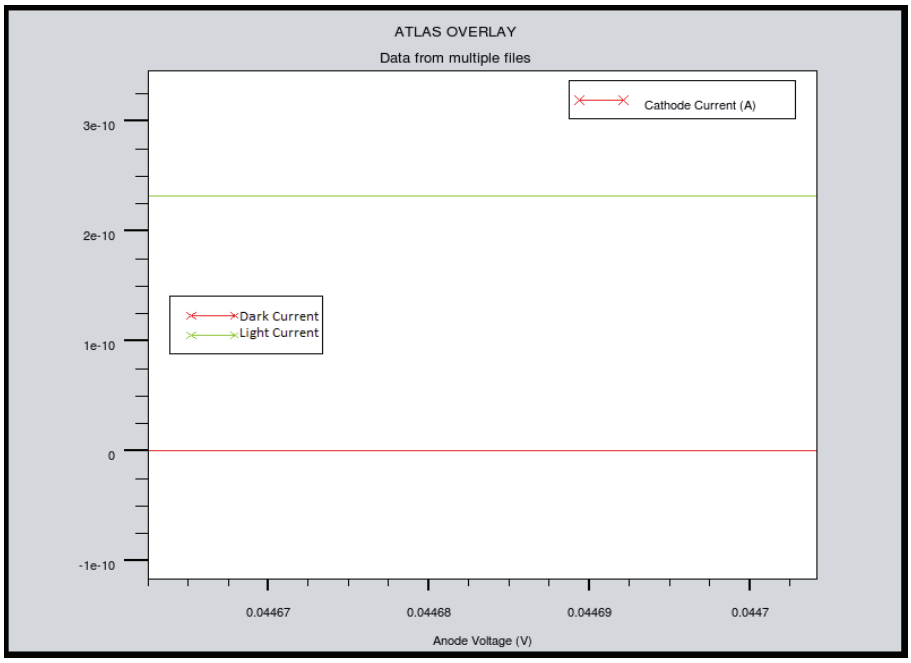

Zoomed view of dark current and light current of Device2

Figure 2.8.

2.3.3. Observation:

Short Circuit Current,
Isc: 2.3246×10^{-10}A
Efficiency, Eff: 2.87003%

2.4. Comparing Device1 and Device2

2.4.1. Comparing Photogeneration

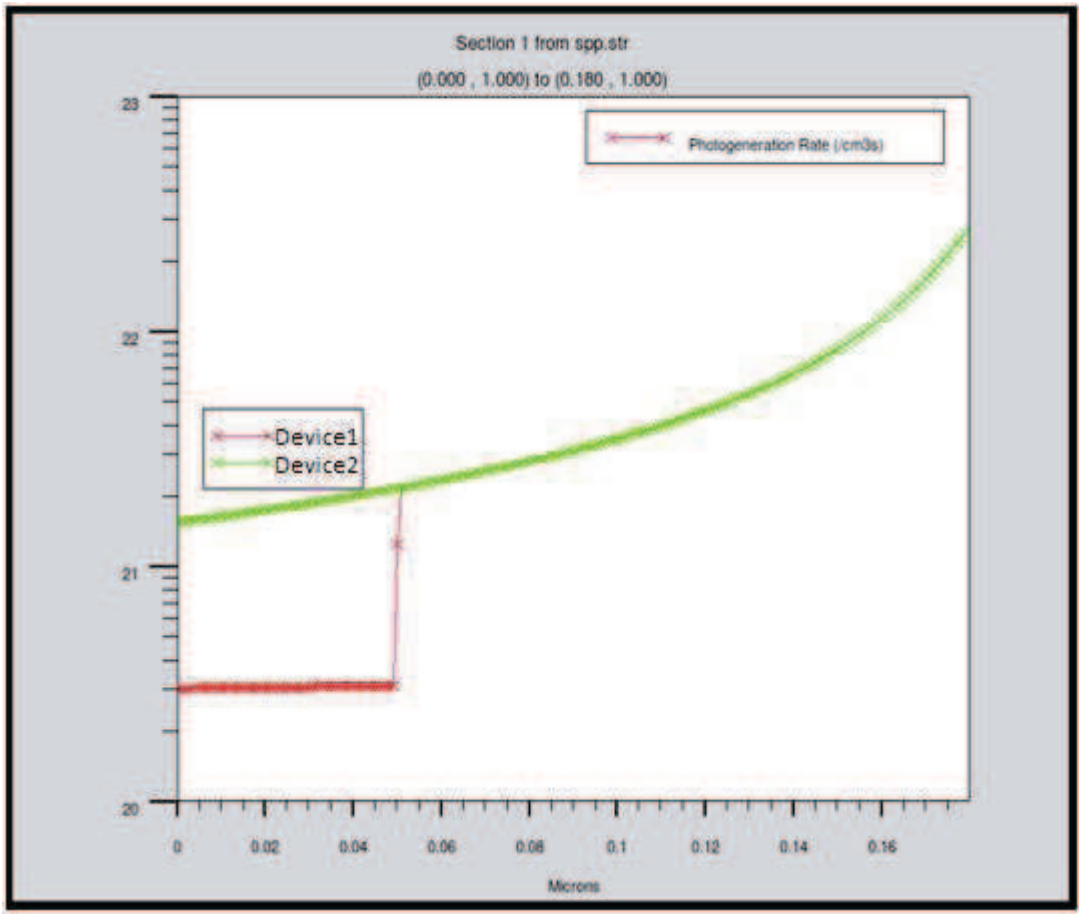

Radial Photo generation in Device1 and Device2

Figure2.9.

Comment:

It can be seen in the Figure 2.9. that the photogeneration rate in the p-region in both the devices vary, whereas that in the i-type and n-type region is same. Thus it is seen that the photogeneration in crystalline silicon is less than that in the polysilicon.

2.4.2. Comparing Potential Profile

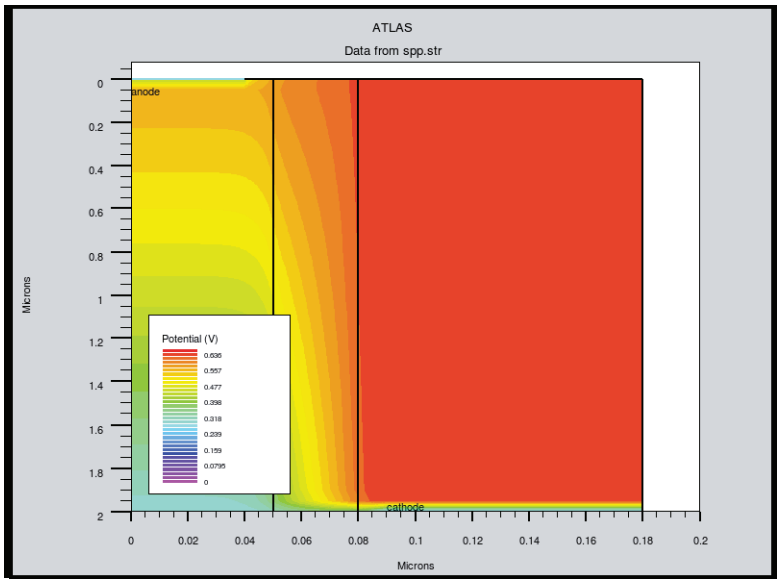

Potential Profile of Device1

Figure 2.10.

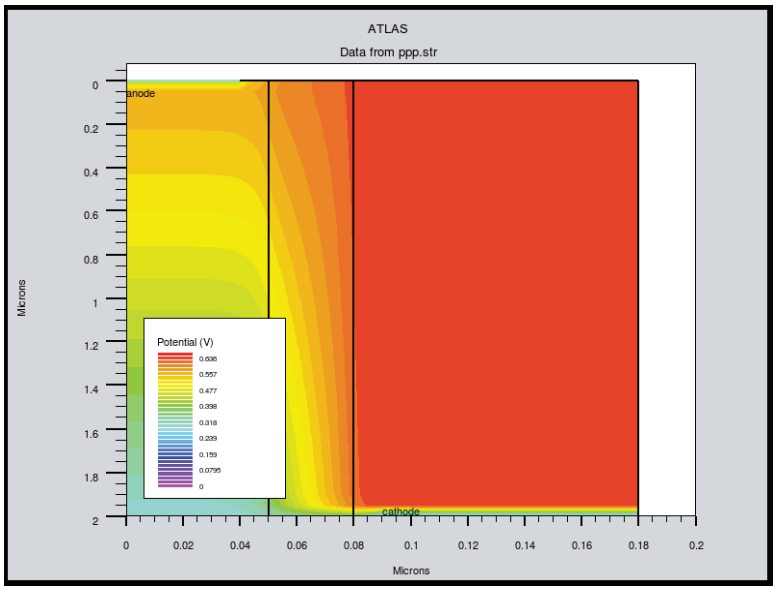

Potential Profile of Device2

Figure 2.11.

Comment:

Potential profile of both the devices are same.

2.4.3. Comparing built in electric field

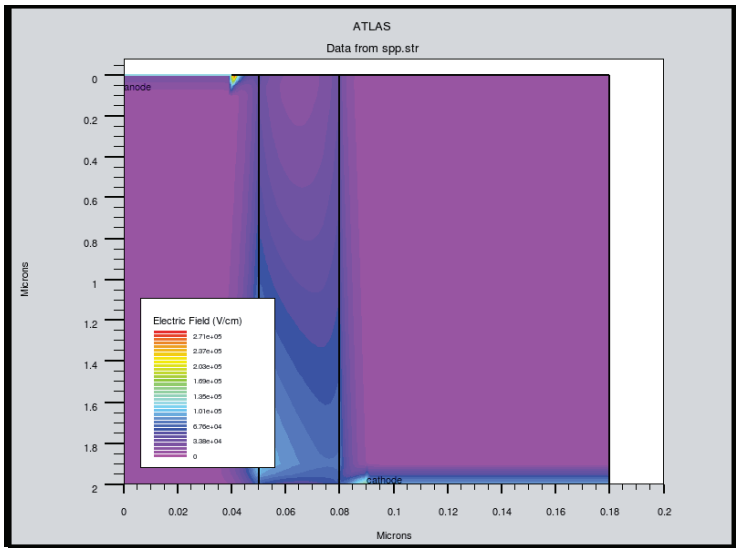

In built electric field in Device1

Figure 2.12.

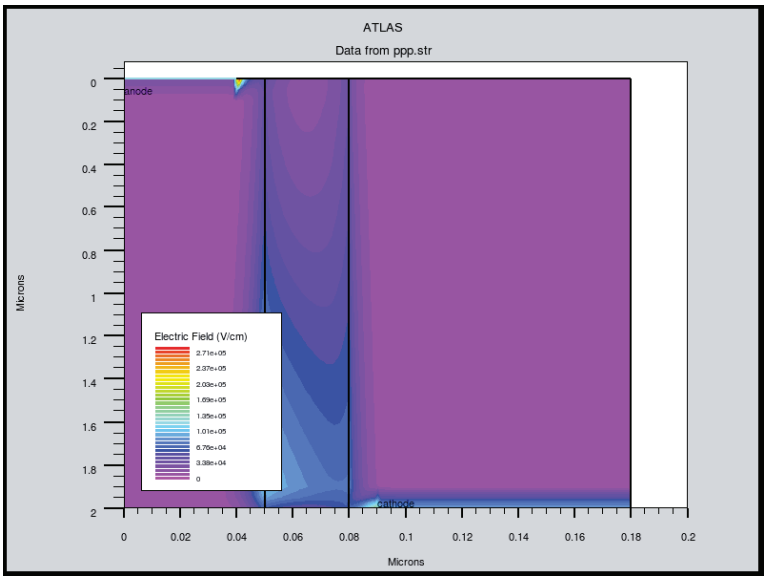

In built electric field in Device2

Figure 2.13.

Comment:

The in-built electric field in Device1 and Device2 is same.

2.4.4. Comparing recombination in device

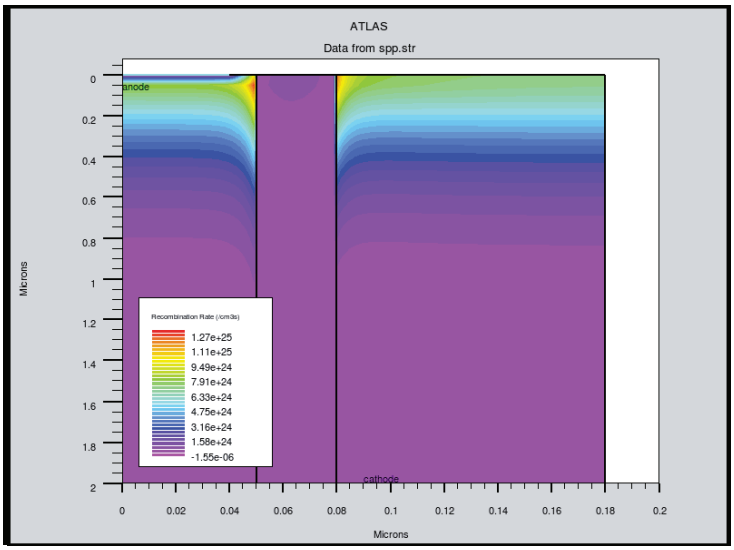

Recombination rate in device1

Figure 2.14.

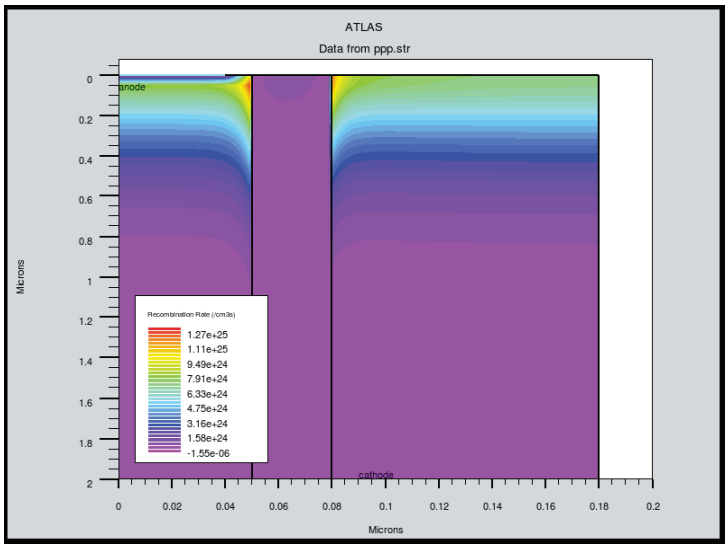

Recombination Rate inDevice2

Figure 2.15.

Comment:

The recombination rate in both the devices is same.

2.4.5. Other parameter comparison:

	Device1	Device2	Difference	% Difference
Isc	2.28424×10^{-10} A	2.3246×10^{-10}A	4.04E-12A	1.77%
Eff	2.81652%	2.87003%	5.35E-02A	1.90%

Comment:

It is observed that the Current and Efficiency is increased in Device2 as compared to Device1 by 1.77% and 1.90% respectively.

2.4.6 Inference:

As it is observed, potential gradient, recombination rate, electric field in both the devices is identical, the only difference occurs in photogeneration rate in the p-type region in both the cells.

It is seen that photogeneration is higher in the polysilicon than in crystalline silicon p-type region. This contributes to higher current and thus in higher efficiency of device2 as compared to device1.

Thus it can be inferred that a coaxial nanowire solar cell made completely of polysilicon is more efficient than the cell in which the p-type material is crystalline silicon and i-type and n-type are polysilicon.

2.5. Effect of variation of intrinsic layer thickness

Keeping the diameter of the solar cell constant, that is, 360 nm, the thickness of the intrinsic layer is varied from 28nm to 40 nm in the steps of 2 nm.

As the thickness of the intrinsic layer is increased by a step of 2nm, 1 nm is reduced in the radius of the p-type cylinder, and 1 nm is reduced in the thickness of n type layer

Thus there are the following variations:

Device Name	Radius of p-type cylinder	Thickness of i-type Layer	Thickness of n-type Layer
Device 3a	51nm	28nm	101mn
Device 3b	50nm	30nm	100nm
Device 3c	49nm	32nm	99nm
Device 3d	48nm	34nm	98nm
Device 3e	47nm	36nm	97nm
Device 3f	46nm	38nm	96nm
Device 3g	45nm	40nm	95nm

2.5.1. Various Structures:

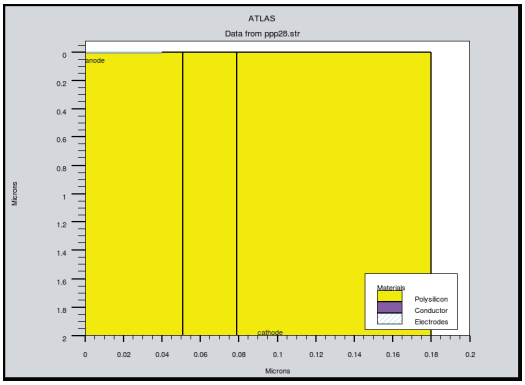

i-thickness=28nm

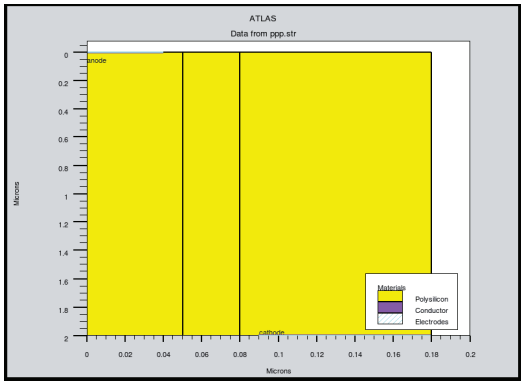

i-thickness=30nm

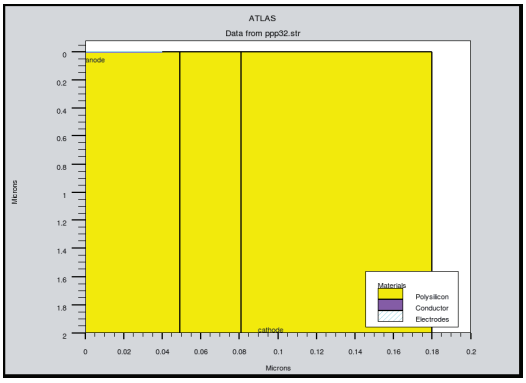

i-thickness=32nm

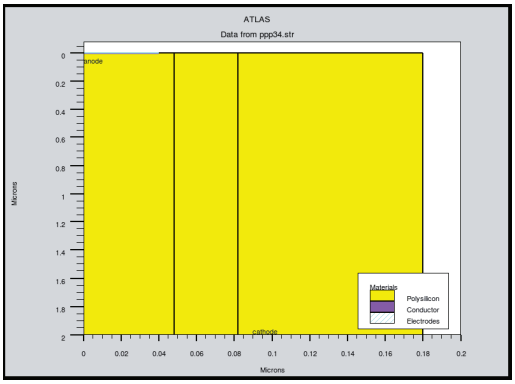

i-thickness=34nm

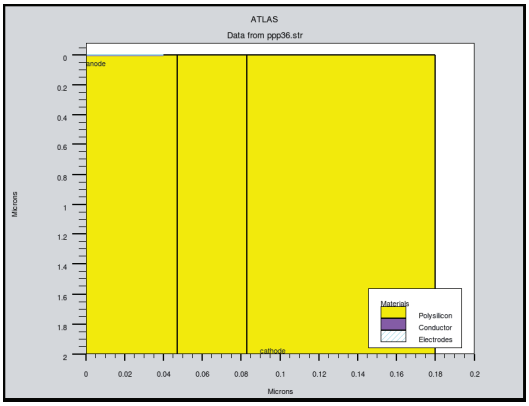

i-thickness=36nm

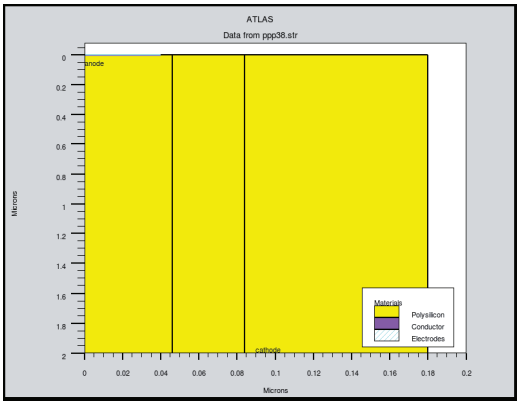

i-thickness=38nm

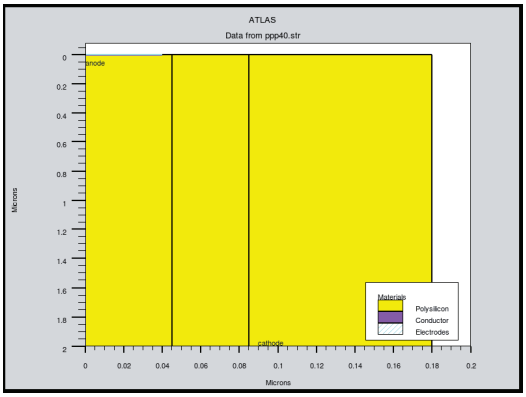

i-thickness=40nm

Structure of Device 3a-3g

Figure 2.16

2.5.2. Dark-Current Characteristics:

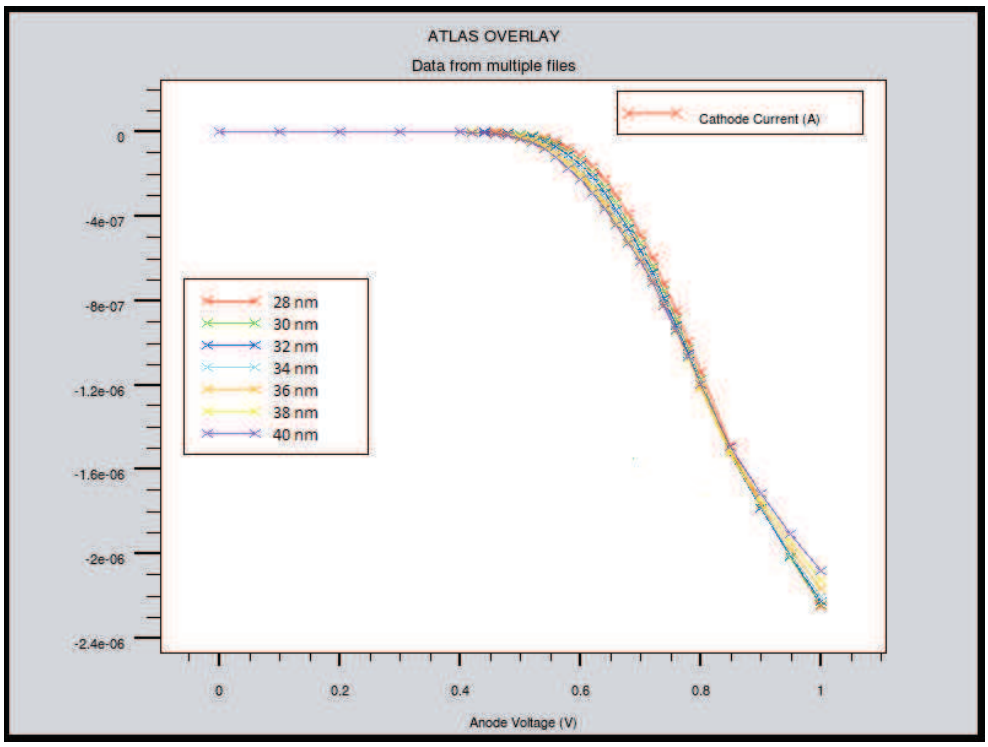

Dark-Current Characteristic of Device 3a-3g

Figure 2.17.

Comment:

As the i-layer thickness increases, voltage at which the cell turns on in the unilluminated condition, Vt, reduces.

2.5.3. Light-Current Characteristics:

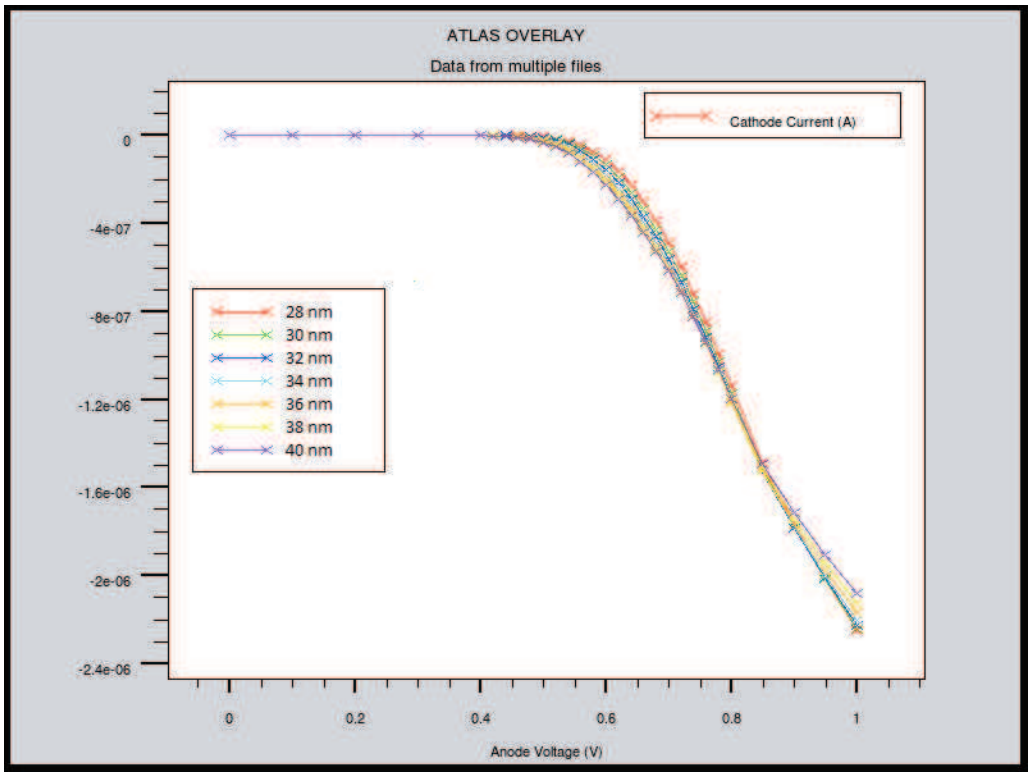

Light-Current Characteristic of Device 3a-3g
Figure 2.18.

Comment:

As the i-layer thickness increases, voltage at which the cell turn on under illumination, Vt_ill, reduces.

2.5.4. Photogeneration rate in the device:

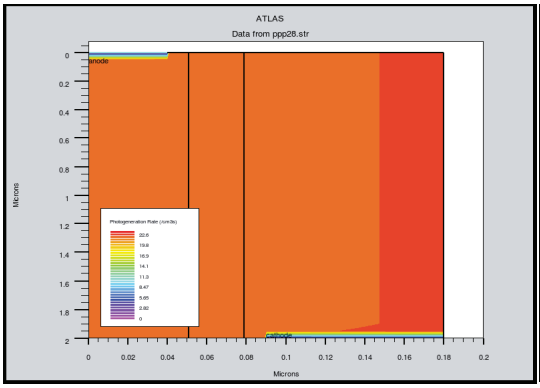

i-thickness=28nm

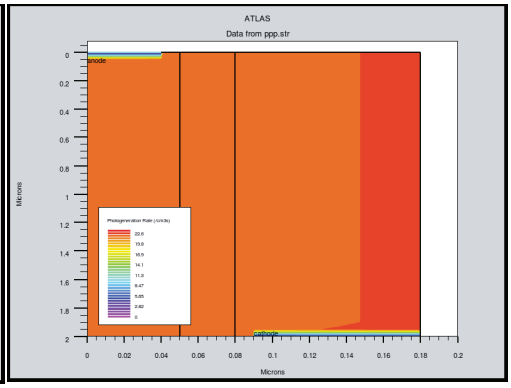

i-thickness=30nm

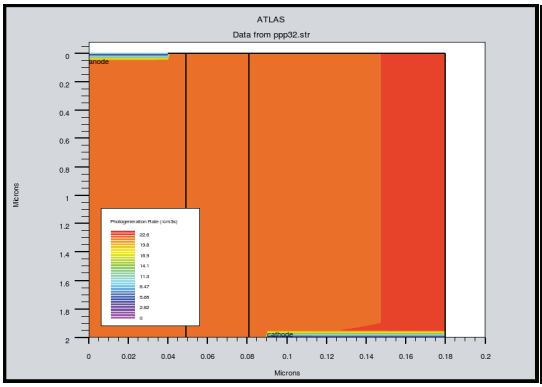

i-thickness=32nm

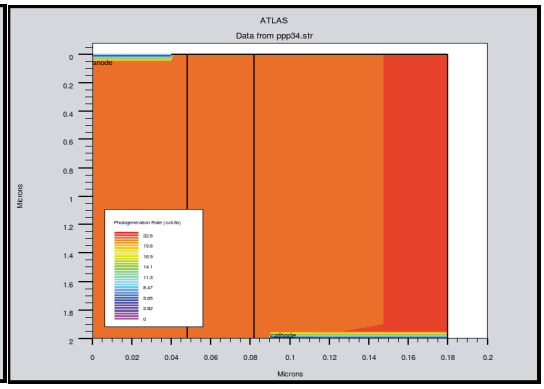

i-thickness=34nm

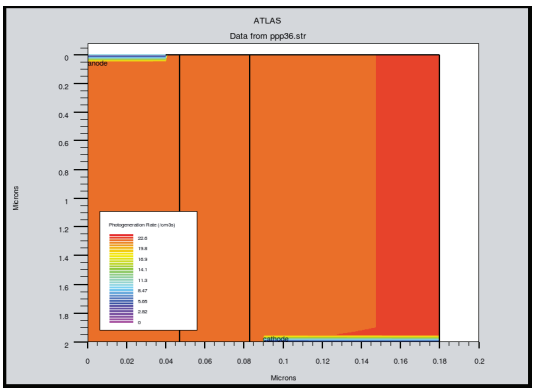

i-thickness=36nm

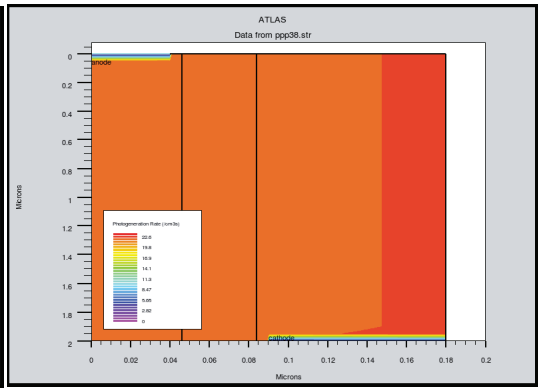

i-thickness=38nm

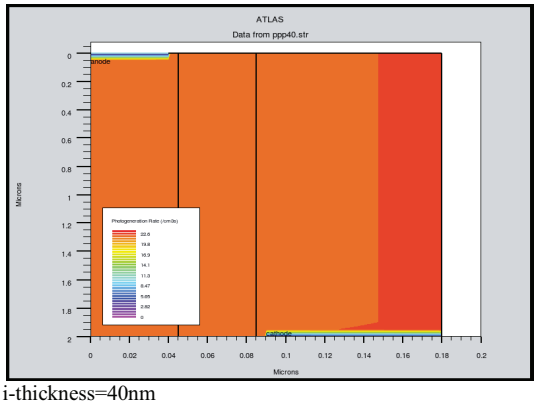

i-thickness=40nm

Comment:

It is observed that the photogeneration is same in all variations

Photogeneration in Device 3a-3g

Figure 2.19.

2.5.5. Photogeneration at anode:

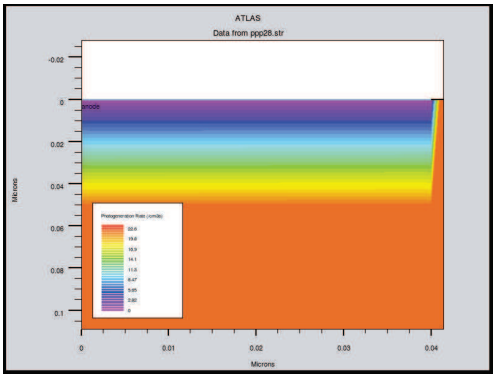

i-thickness=28nm

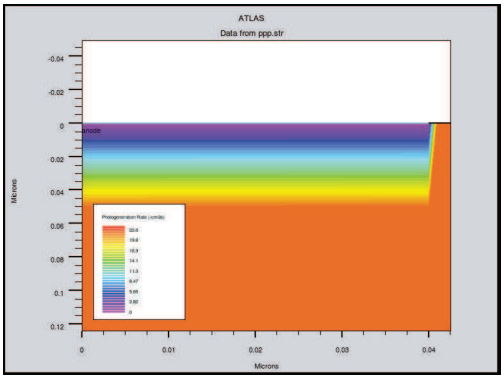

i-thickness=30nm

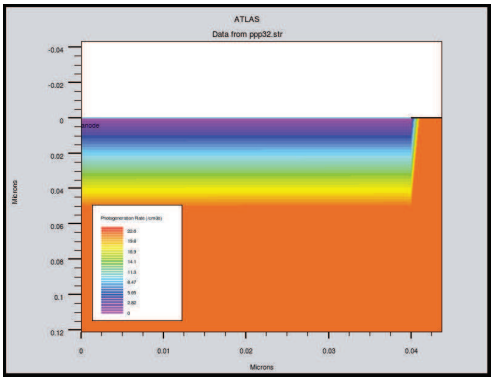

i-thickness=32nm

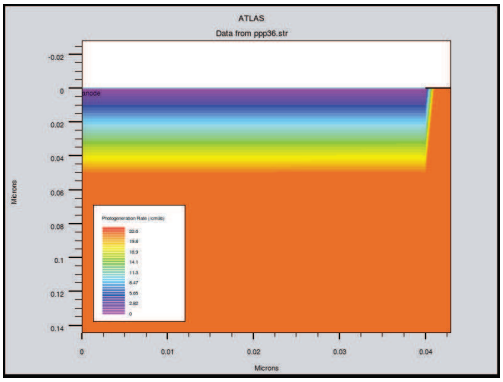

i-thickness=34nm

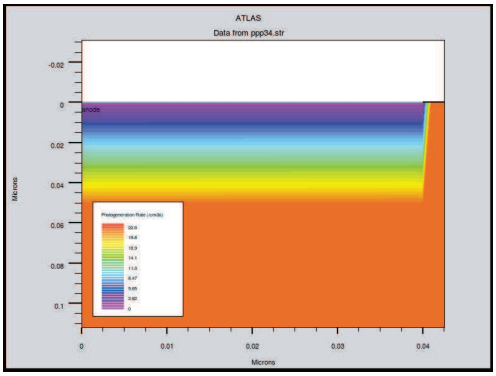

i-thickness=36nm

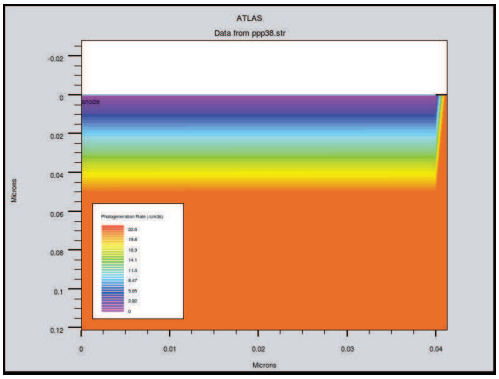

i-thickness=38nm

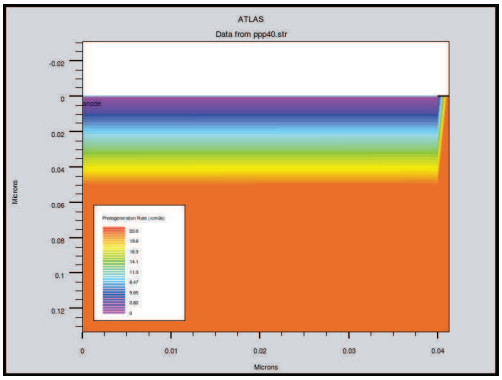

i-thickness=40nm

Photogeneration at anode in Device 3a-3g

Figure 2.20.

2.5.6. Photogeneration at cathode:

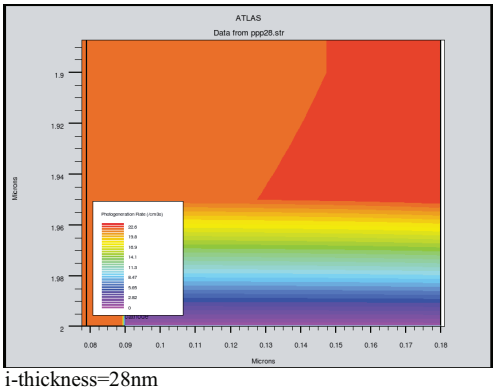

i-thickness=28nm

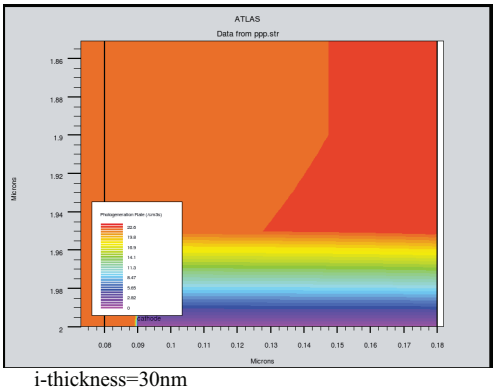

i-thickness=30nm

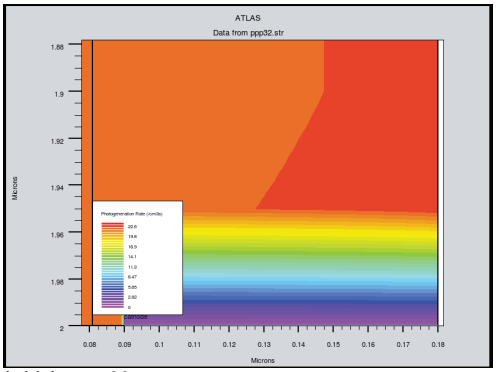

i-thickness=32nm

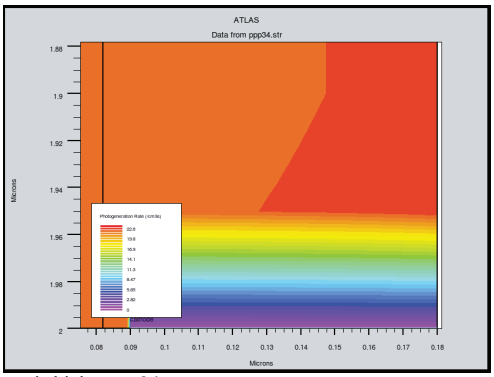

i-thickness=34nm

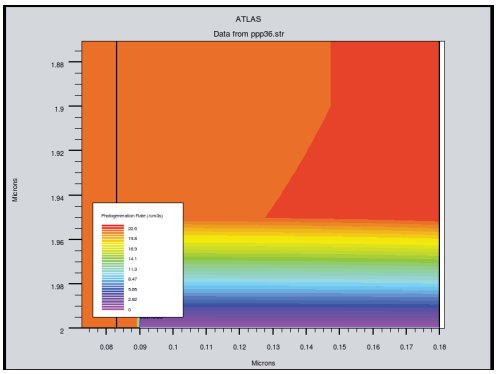

i-thickness=36nm

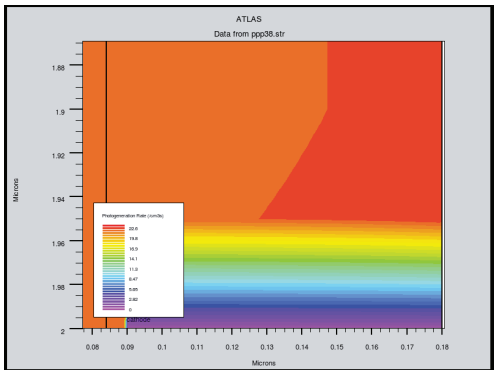

i-thickness=38nm

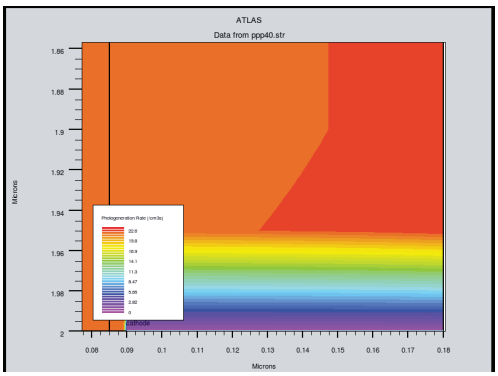

i-thickness=40nm

Photogeneration at cathode in Device 3a-3g

Figure 2.21

2.5.7. Potential profile:

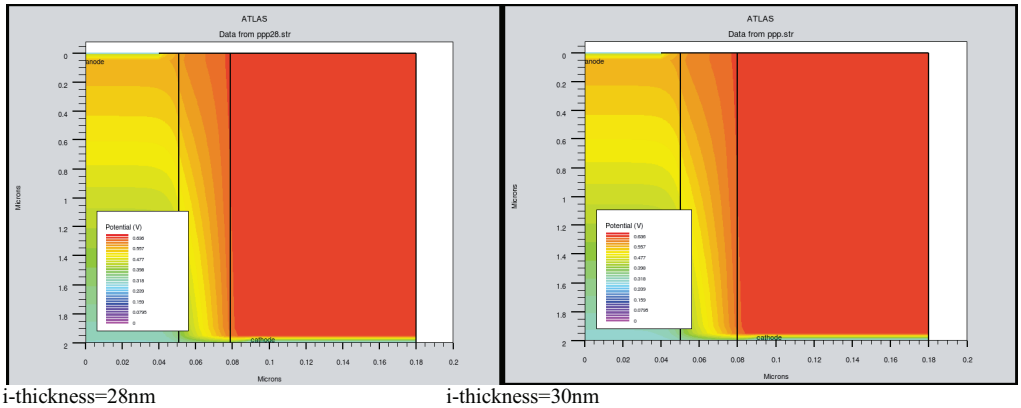

i-thickness=28nm i-thickness=30nm

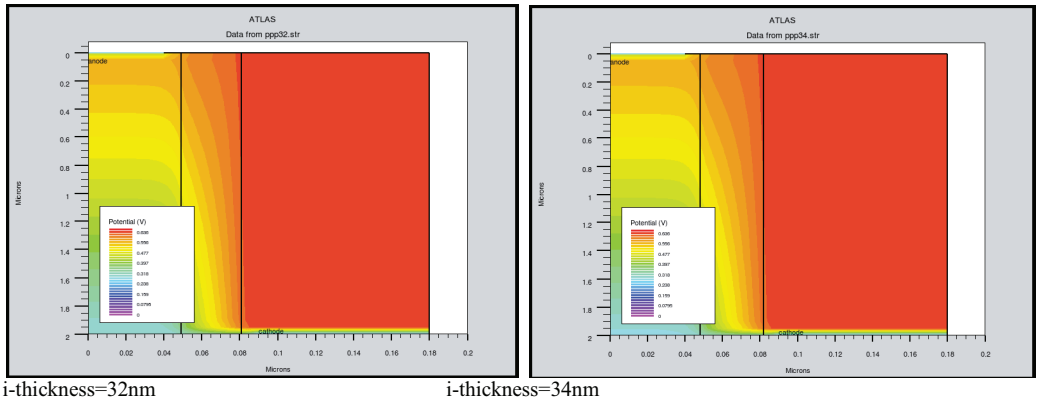

i-thickness=32nm i-thickness=34nm

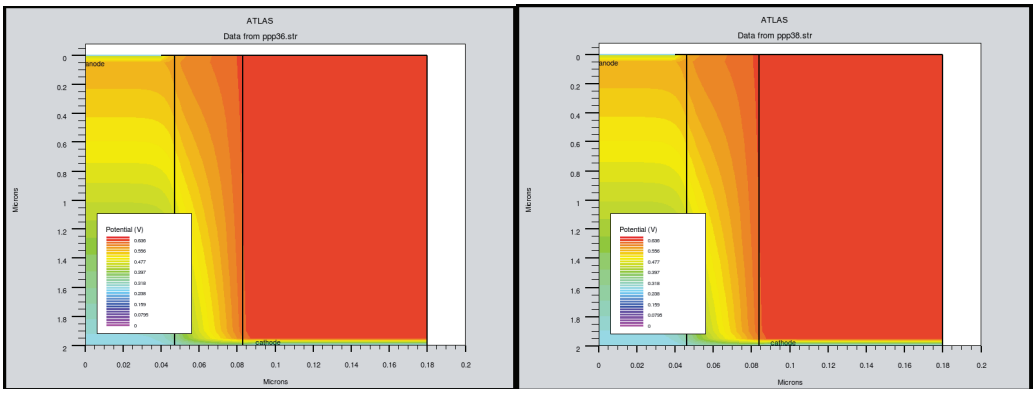

i-thickness=36nm i-thickness=38nm

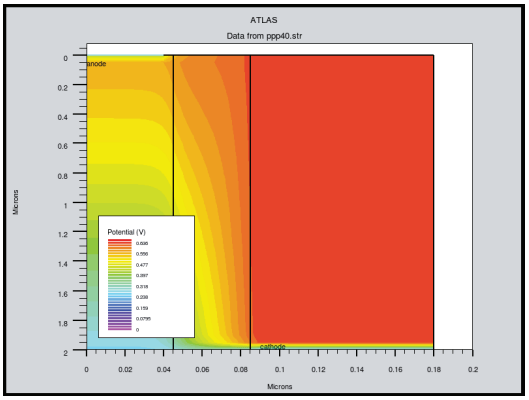

i-thickness=40nm

Comment:

It is observed that as the i-layer thickness increases, the steepness of the potential gradient decreases.

Potential Profile in Device 3a-3g

Figure 2.22.

2.5.8. Comparing Photogeneration in radial direction at y=1 micron

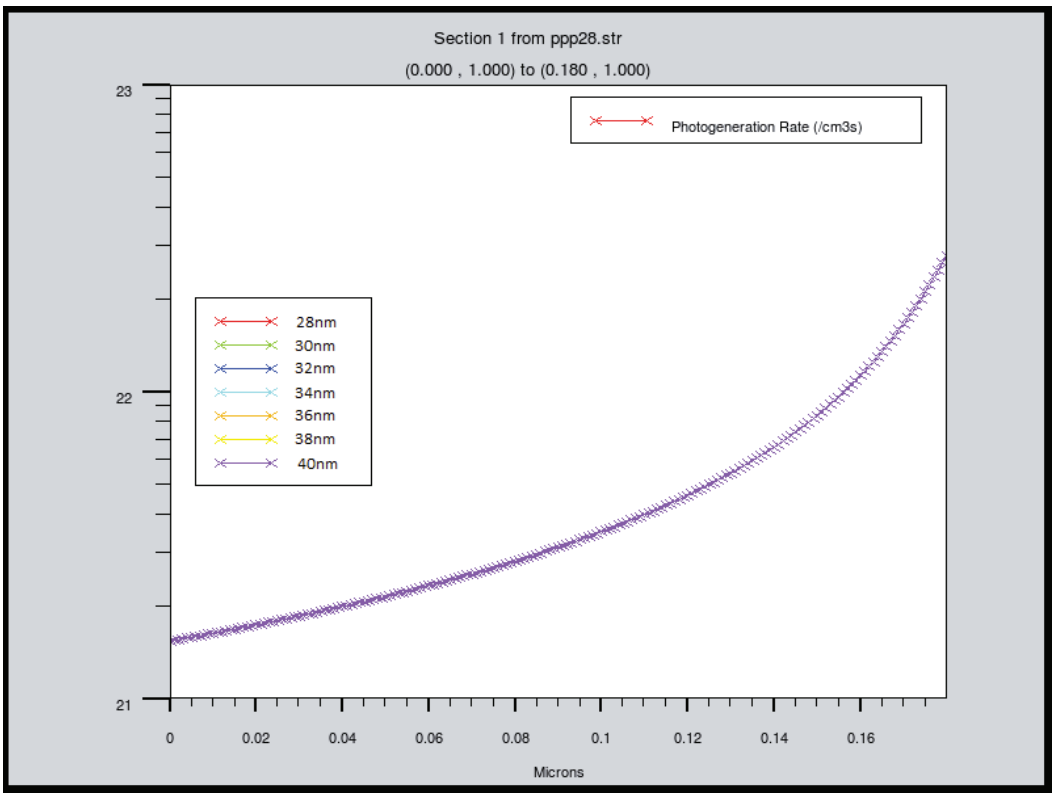

Photogeneration in radial direction at y=1 micron in Device 3a-3g

Figure2.23.

Comment:

Photogeneration in the radial direction at y=1 micron, remains the same irrespective of the thickness of the i-layer.

2.5.9. Recombination in the device:

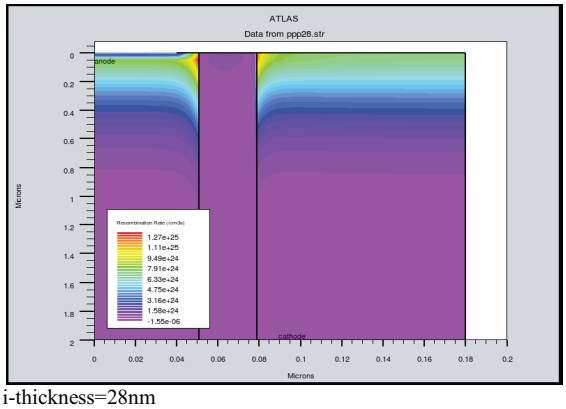

i-thickness=28nm

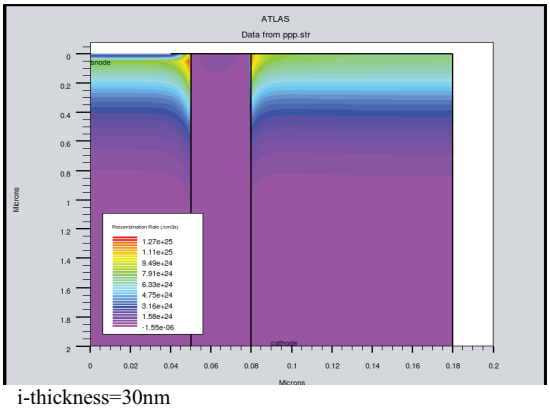

i-thickness=30nm

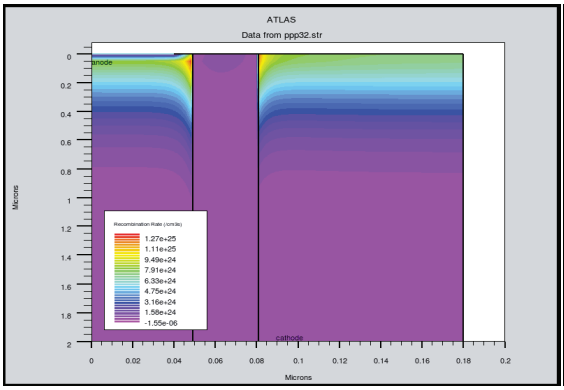

i-thickness=32nm

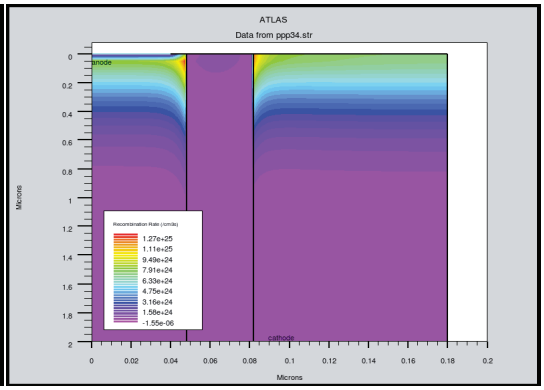

i-thickness=34nm

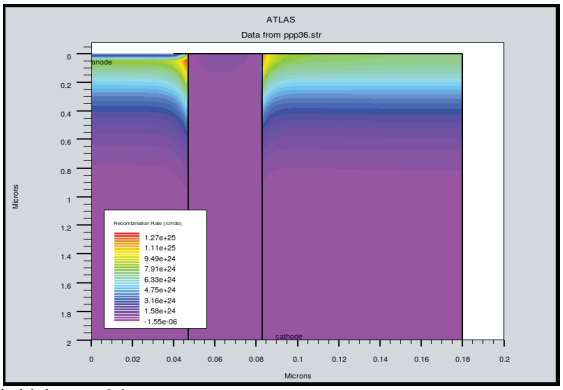

i-thickness=36nm

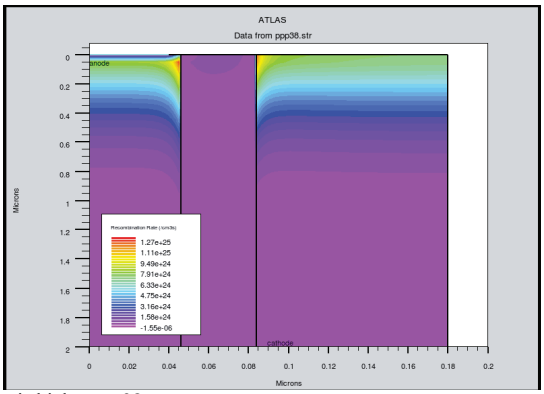

i-thickness=38nm

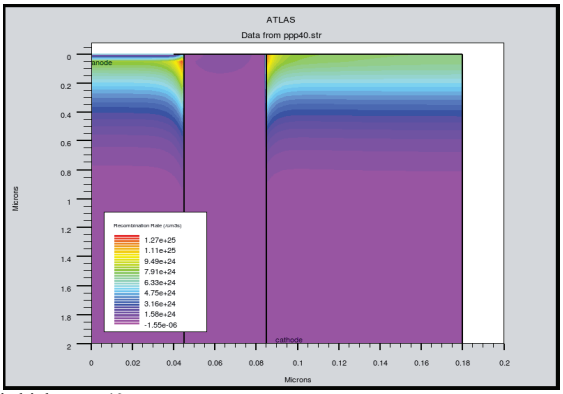

i-thickness=40nm

Comment:

It is observed that the recombination is higher in the p-type and n-type region than in the i-type region. Thus as the i-thickness is increased, the p-type and n-type region is reduced, therefore the overall recombination is reduced.

Recombination in Device 3a-3g

Figure 2.24.

2.5.10. Various Parameters Observed:

i-thickness	28nm	30nm	32nm	34nm	36nm	38nm	40nm
p-radius	51nm	50nm	49nm	48nm	47nm	46nm	45nm
n-thickness	101nm	100nm	99nm	98nm	97nm	96nm	95nm
Isc(A)	2.324E-10	2.325E-10	2.325E-10	2.326E-10	2.327E-10	2.328E-10	2.329E-10
Voc(V)	0.366208	0.349962	0.337704	0.328581	0.321923	0.316999	0.313406
Pm(W)	6.590E-11	6.494E-11	6.372E-11	6.224E-11	6.048E-11	5.843E-11	5.621E-11
Vm(V)	0.3	0.3	0.3	0.3	0.3	0.3	0.3
Im(A)	2.197E-10	2.165E-10	2.124E-10	2.075E-10	2.016E-10	1.948E-10	1.874E-10
Eff	2.91239	2.87003	2.81614	2.75072	2.67284	2.58228	2.4841
Vt(V)	0.646213	0.639243	0.632846	0.627502	0.623172	0.619773	0.617244
Vt_ill(V)	0.64628	0.639318	0.632928	0.62759	0.623266	0.619872	0.61735

The following variations can be observed in the above table with respect to the thickness of i-layer:

Short Circuit Current, Isc:

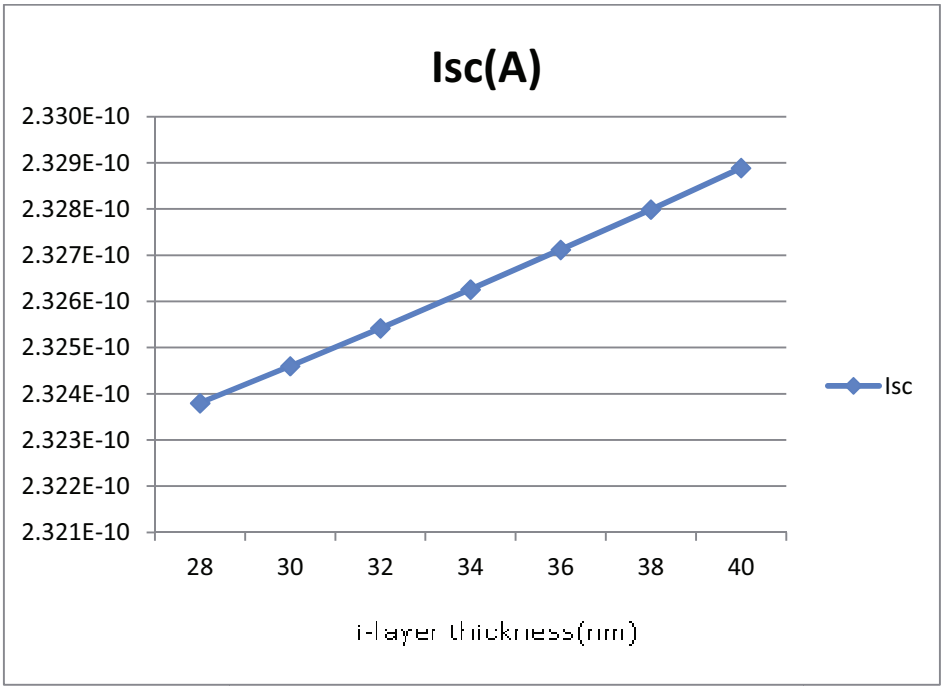

Impact of variation of i-layer thickness on Isc
Figure 2.25.

Open Circuit Voltage, Voc:

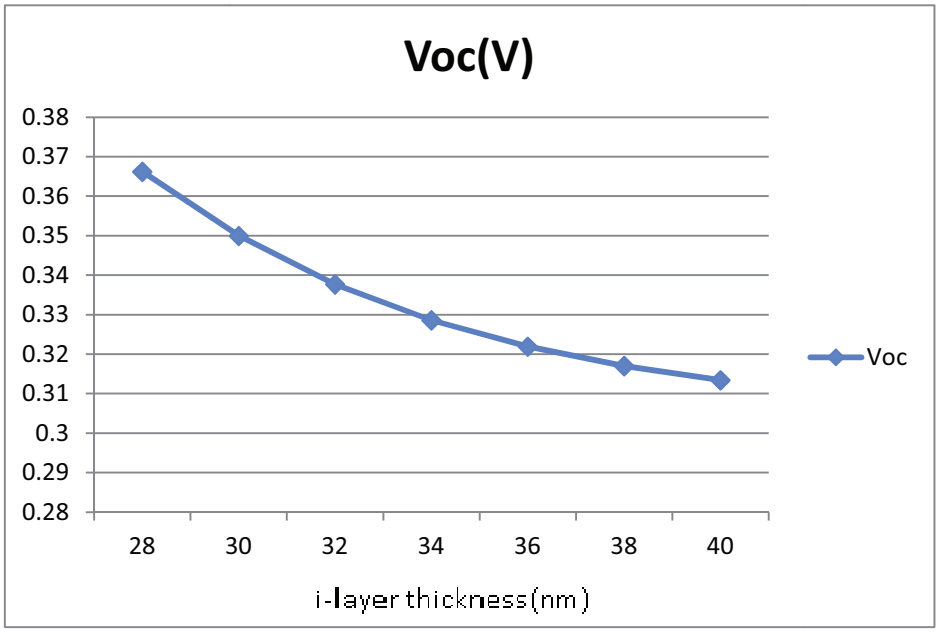

Impact of variation of i-layer thickness on Voc
Figure 2.26.

Maximum Power, Pm:

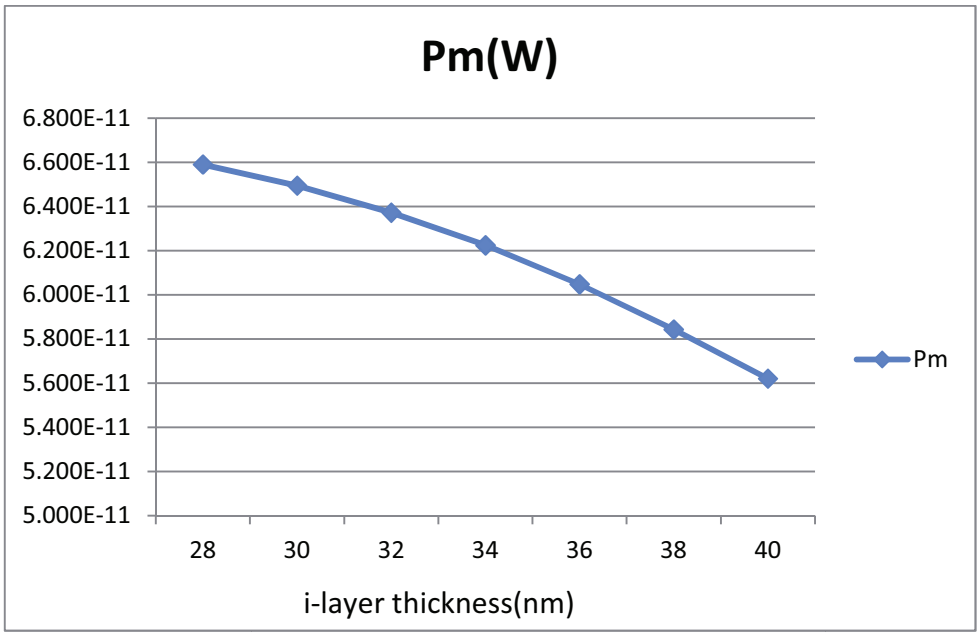

Impact of variation of i-layer thickness on Pm
Figure 2.27

Value of Voltage where Power is maximum, Vm:

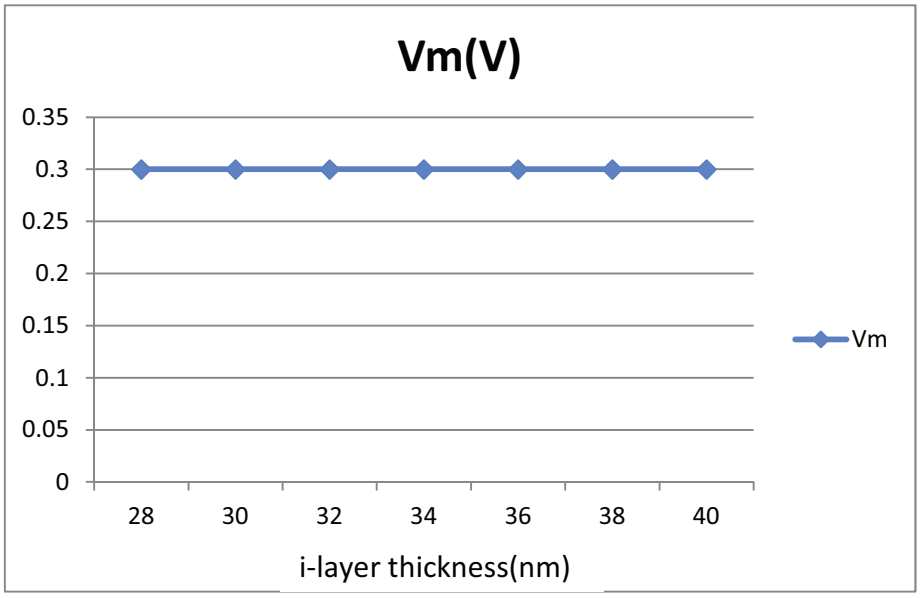

Impact of variation of i-layer thickness on Vm
Figure 2.28.

Value of current where Maximum Power is Generated, Im:

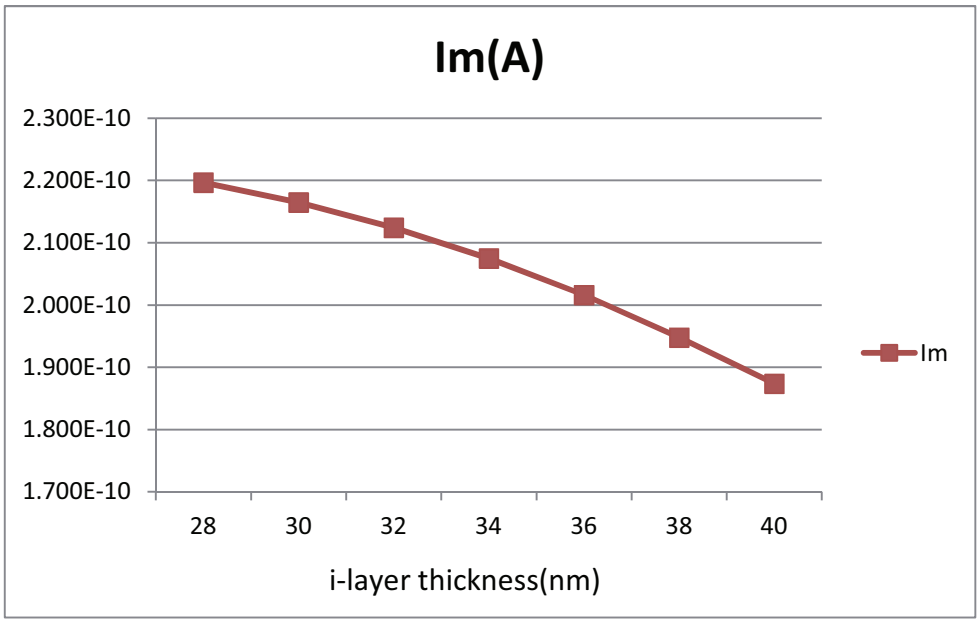

Impact of variation of i-layer thickness on Im
Figure 2.29.

Efficiency, Eff:

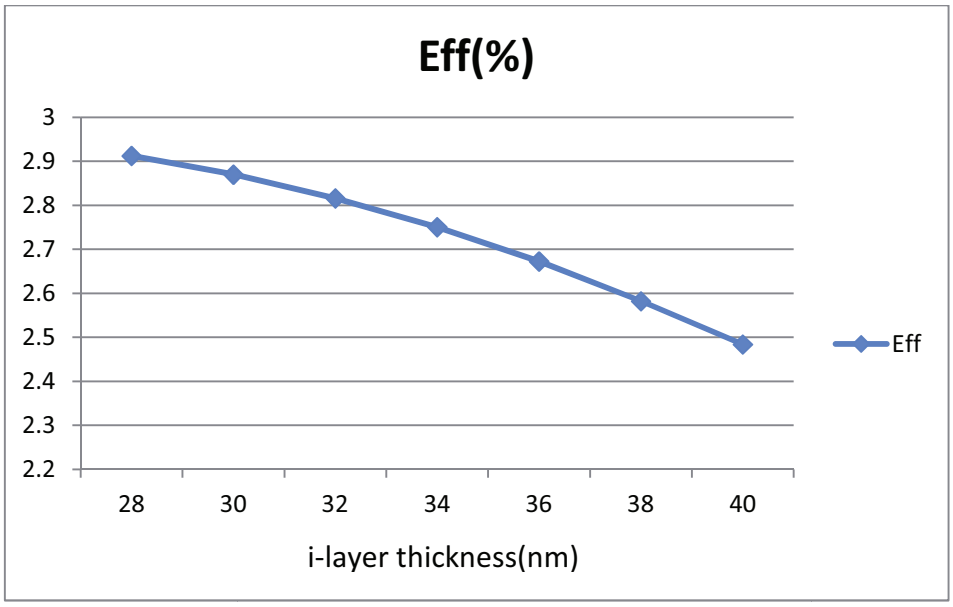

Impact of variation of i-layer thickness on Efficiency
Figure 2.30.

Turn On Voltage under Non-illuminated Condition, Vt:

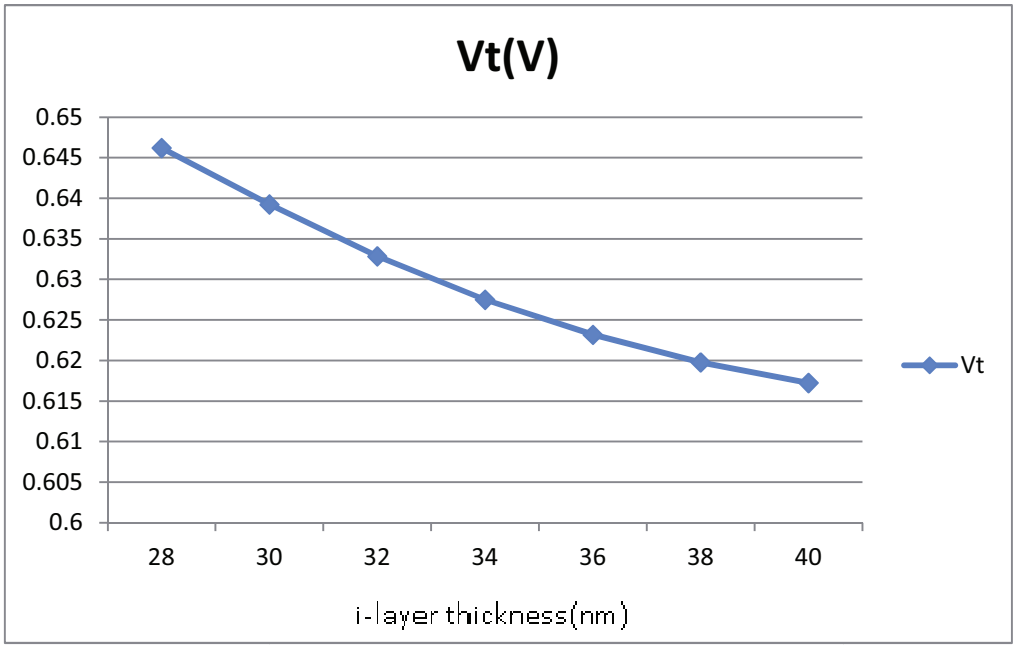

Impact of variation of i-layer thickness on Vt
Figure 2.31.

Turn On Voltage Under illumination: Vt_ill:

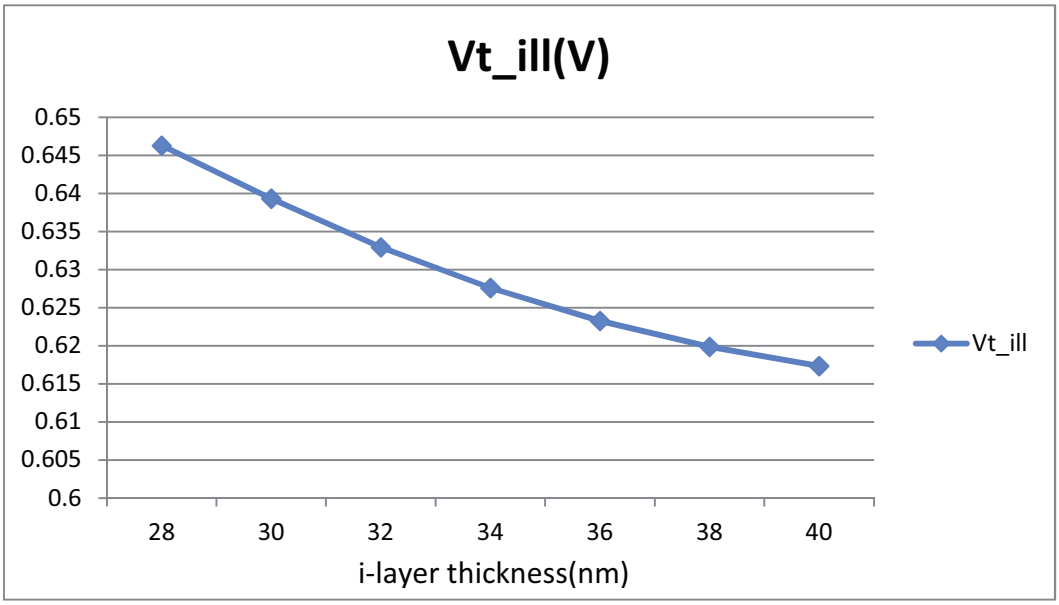

Impact of variation of i-layer thickness on Vt_ill
Figure 2.32

2.5.11. Inferrence:

It has been seen that as the i-layer thickness increases, parameter Isc increases. This can also inferred from the observation that photogeneration in the device is independent of i-layer thickness, where as the over all recombination in the device reduces as the i-layer thickness is increased.

Irrespective of the i-layer thickness, the value of voltage at which the maximum power is generated remains constant, that is, 0.3V.

Other parameters, open circuit voltage, maximum power generated, current at maximum power, efficiency and turn on voltage under unilluminated and illuminated condition reduces as the i-layer thickness increases. The reduction in Voc can be attributed to the fact that with increase in i-layer thickness, the steepness of the potential gradient decreases.

2.6. Effect of variation of the contact metal (work function)

2.6.1. Structure:

The Basic Structure is kept constant as in Device2, only the workfunction of the contacts have been varied.

Thus there are the following variations:

Variation	Work Function of Anode	Work Function of Cathode	Difference in work function
Device4a	4.63 eV	4.53 eV	0.10 eV
Device4b	4.77 eV	4.53 eV	0.24 eV
Device4c	4.8 eV	4.53 eV	0.27 eV
Device4d	5.3 eV	4.63 eV	0.67 eV
Device4e	5.3 eV	4.53 eV	0.77 eV
Device4f	5.3 eV	4.1 eV	1.2 eV

The Basic Structure is shown below:

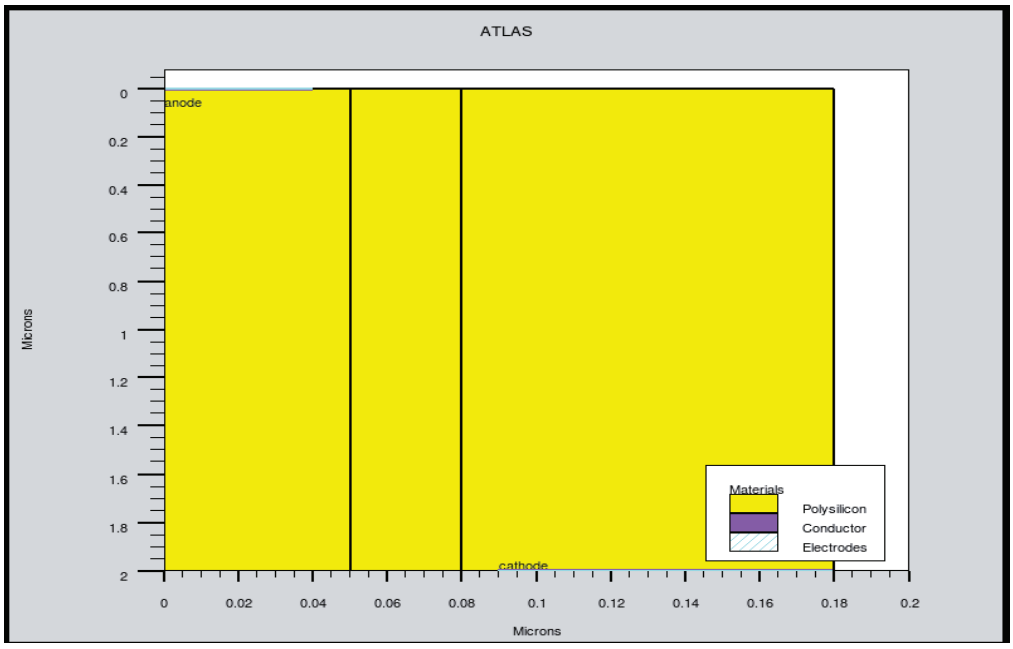

Structure og Device 4a-4f

Figure 2.33.

2.6.2. Dark-Current Characteristics:

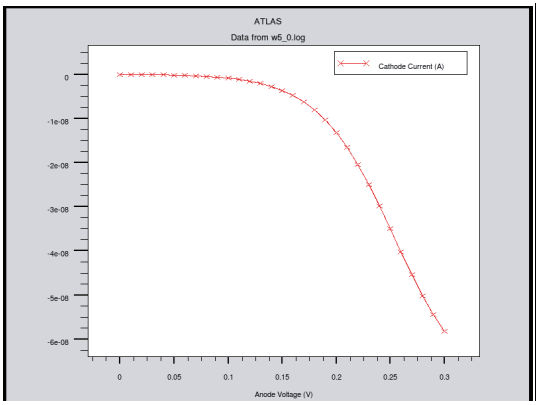

Work Function Difference=0.10eV

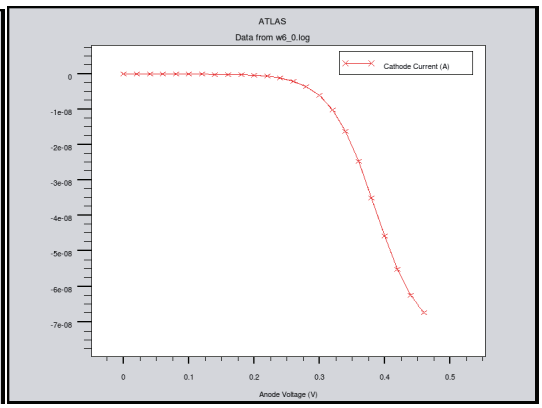

Work Function Difference=0.24eV

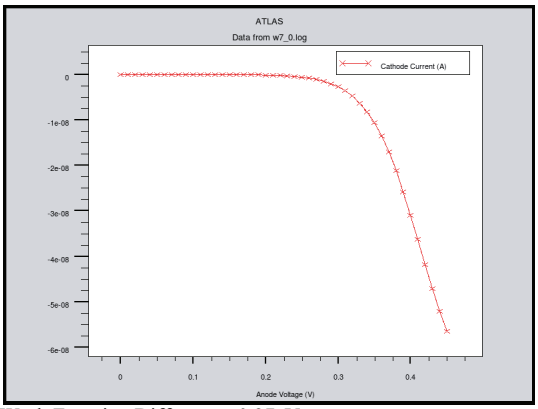

Work Function Difference=0.27eV

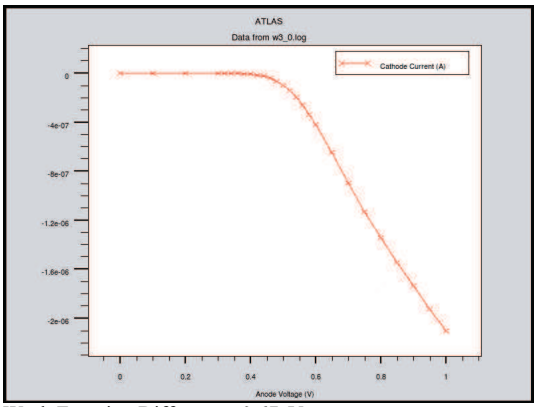

Work Function Difference=0.67eV

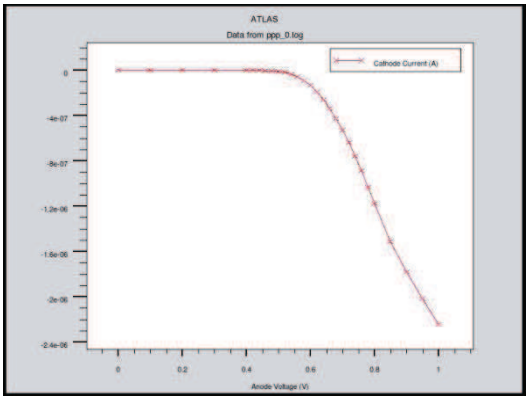

Work Function Difference=0.77eV

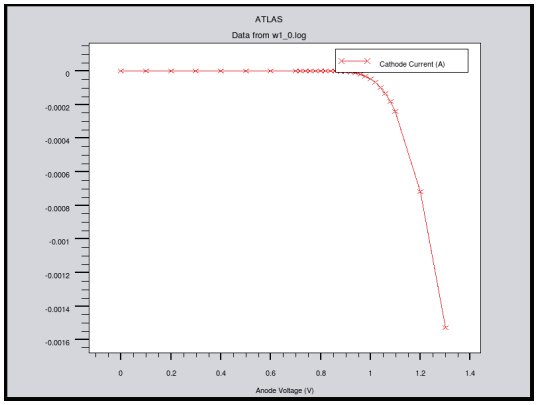

Work Function Difference=1.20eV

Dark-Current Characteristic of Device 4a-4f

Figure 2.34.

2.6.3. Light-Current Characteristics:

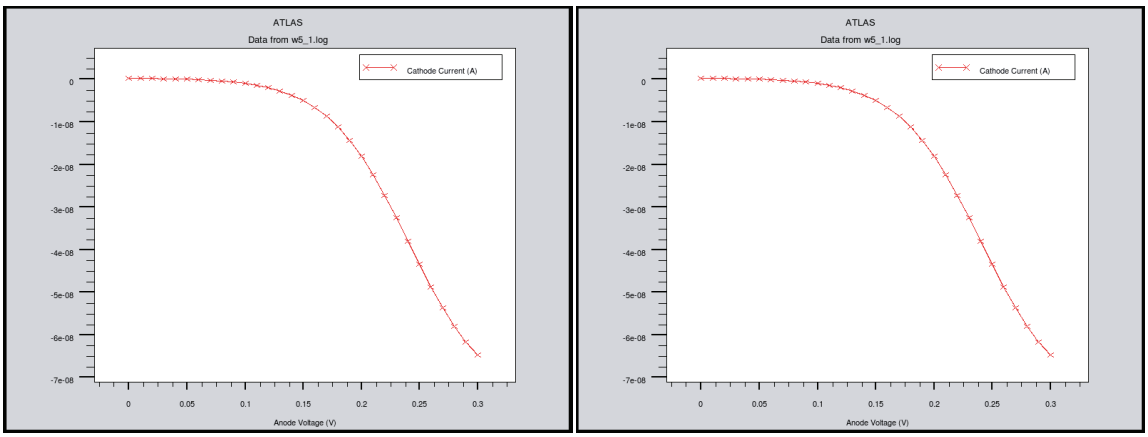

Work Function Difference=0.10eV

Work Function Difference=0.24eV

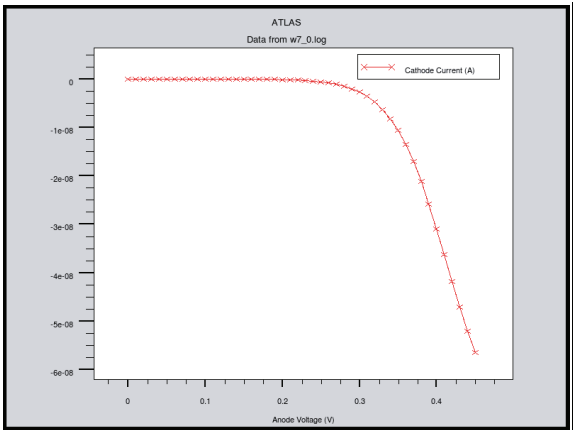

Work Function Difference=0.27eV

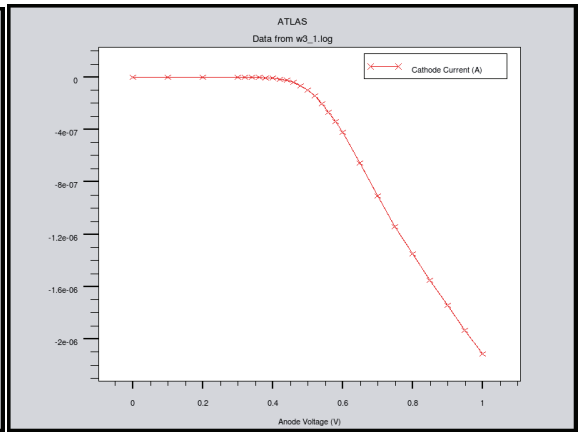

Work Function Difference=0.67eV

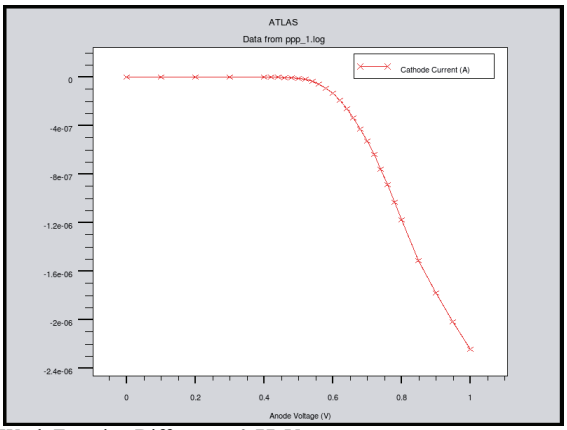

Work Function Difference=0.77eV

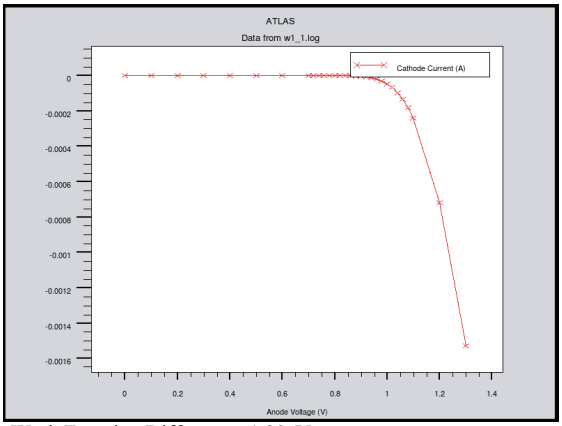

Work Function Difference=1.20eV

Light-Current Characteristic of Device 4a-4f

Figure 2.35.

Comment:

It is observed that as the difference in work function of the electrodes increases, the squareness of the characteristic increases, thus approaching the ideal characteristic.

2.6.4. Photogeneration in the device:

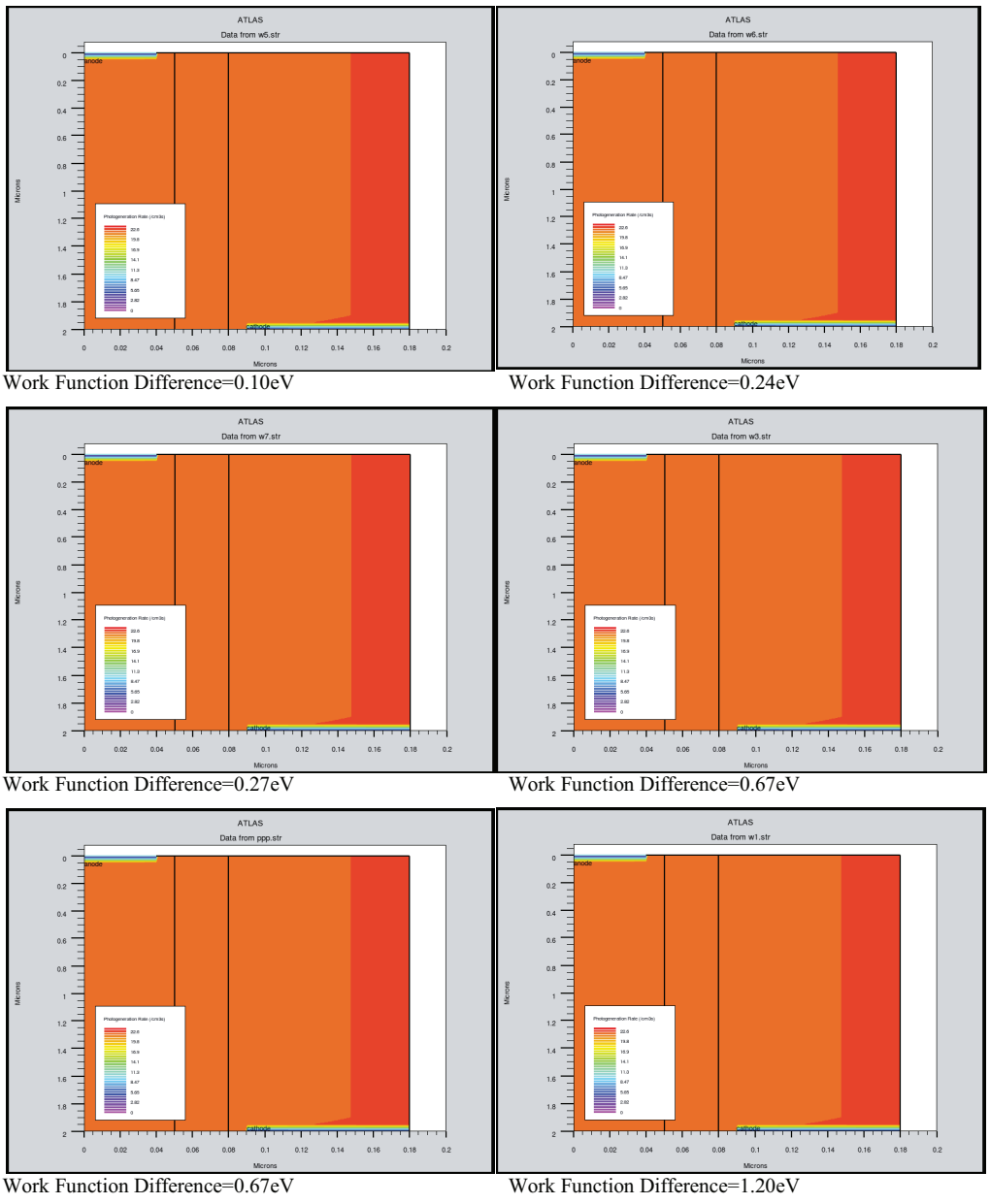

Work Function Difference=0.10eV | Work Function Difference=0.24eV

Work Function Difference=0.27eV | Work Function Difference=0.67eV

Work Function Difference=0.67eV | Work Function Difference=1.20eV

Photogeneration in Device 4a-4f

Figure 2.36.

Comment:

Photogeneration in the device is independent of the variation in the electrode material.

2.6.5. Photogeneration at anode

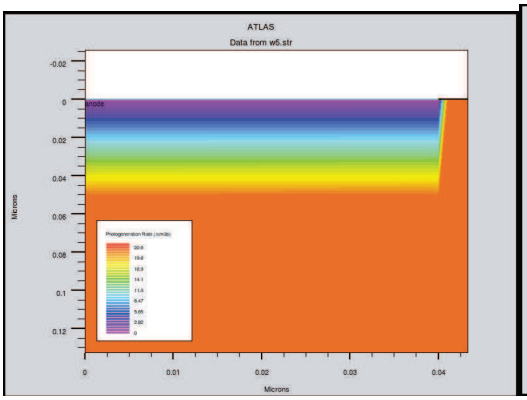

Work Function Difference=0.10eV

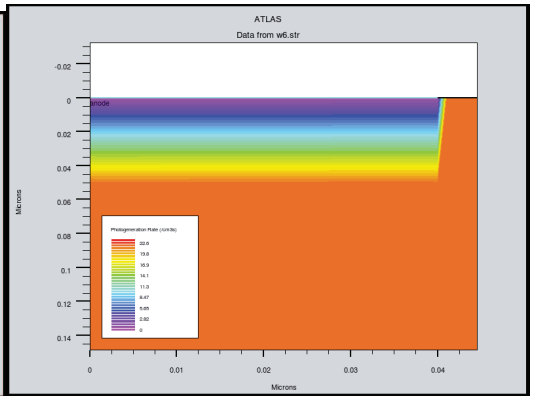

Work Function Difference=0.24eV

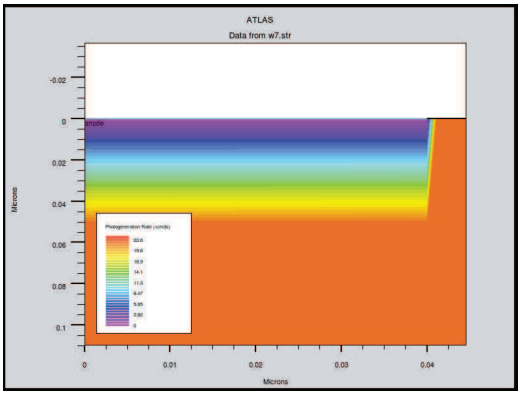

Work Function Difference=0.27eV

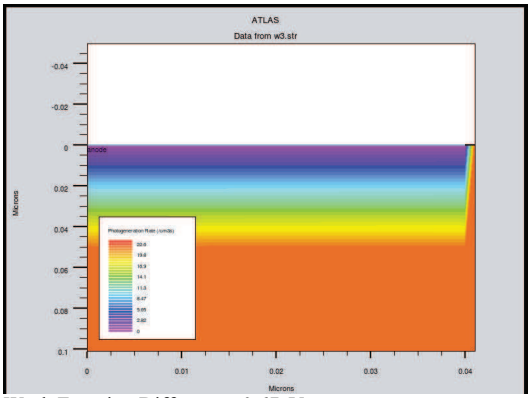

Work Function Difference=0.67eV

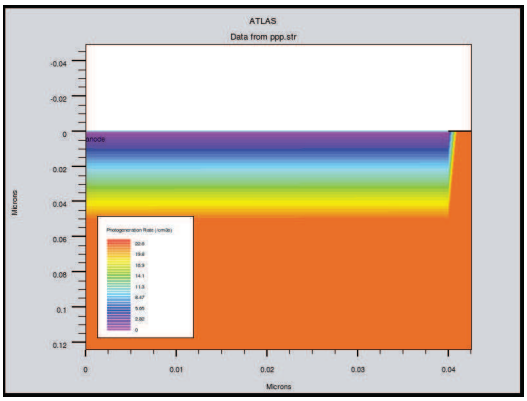

Work Function Difference=0.77eV

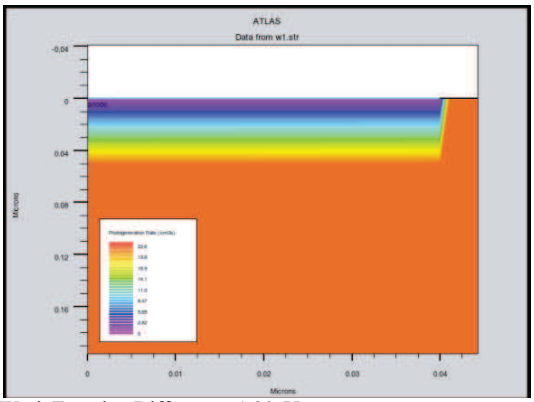

Work Function Difference=1.20eV

Photogeneration at anode in Device 4a-4f

Figure 2.37.

2.6.6. Photogeneration at cathode

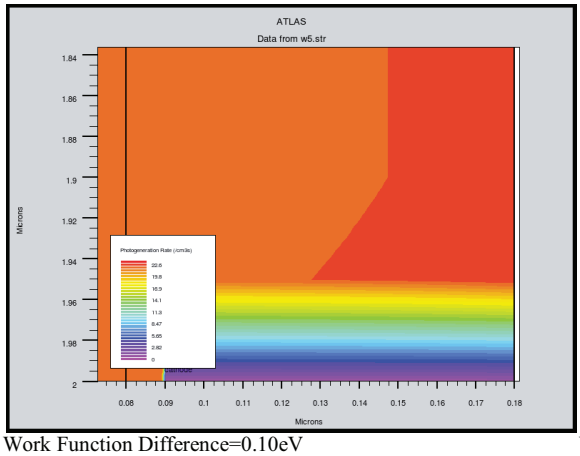

Work Function Difference=0.10eV

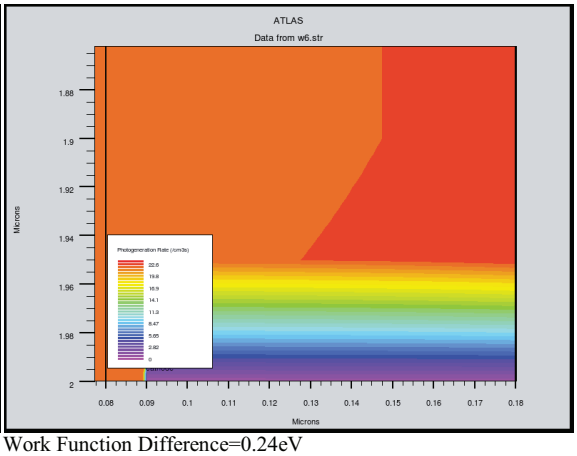

Work Function Difference=0.24eV

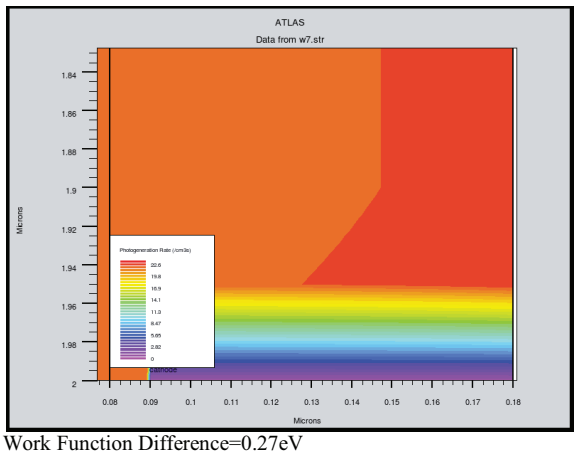

Work Function Difference=0.27eV

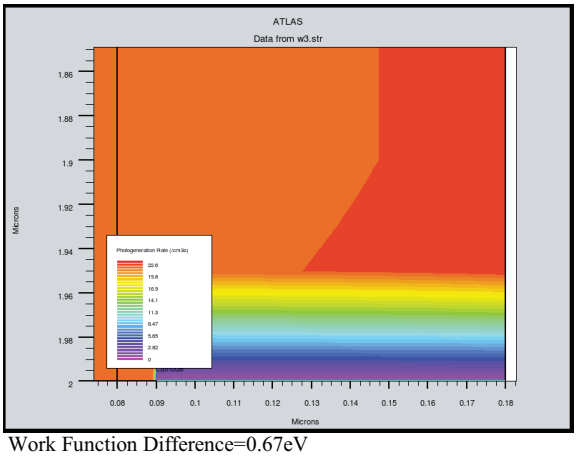

Work Function Difference=0.67eV

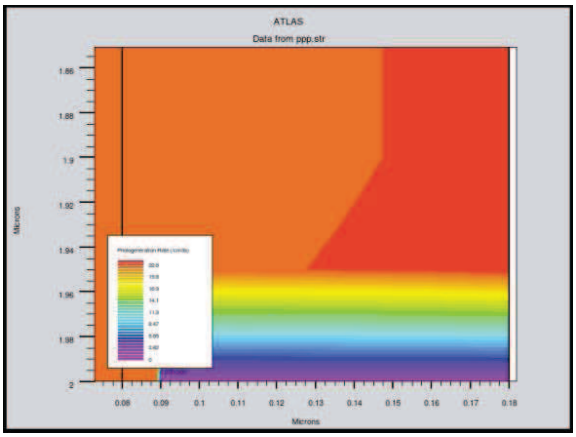

Work Function Difference=0.77eV

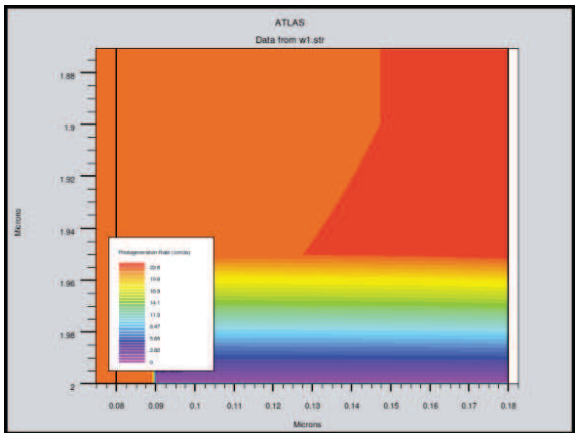

Work Function Difference=1.20eV

Photogeneration at cathode in Device 4a-4f

Figure 2.38.

2.6.7. Photogeneration in radial direction at y=1 micron

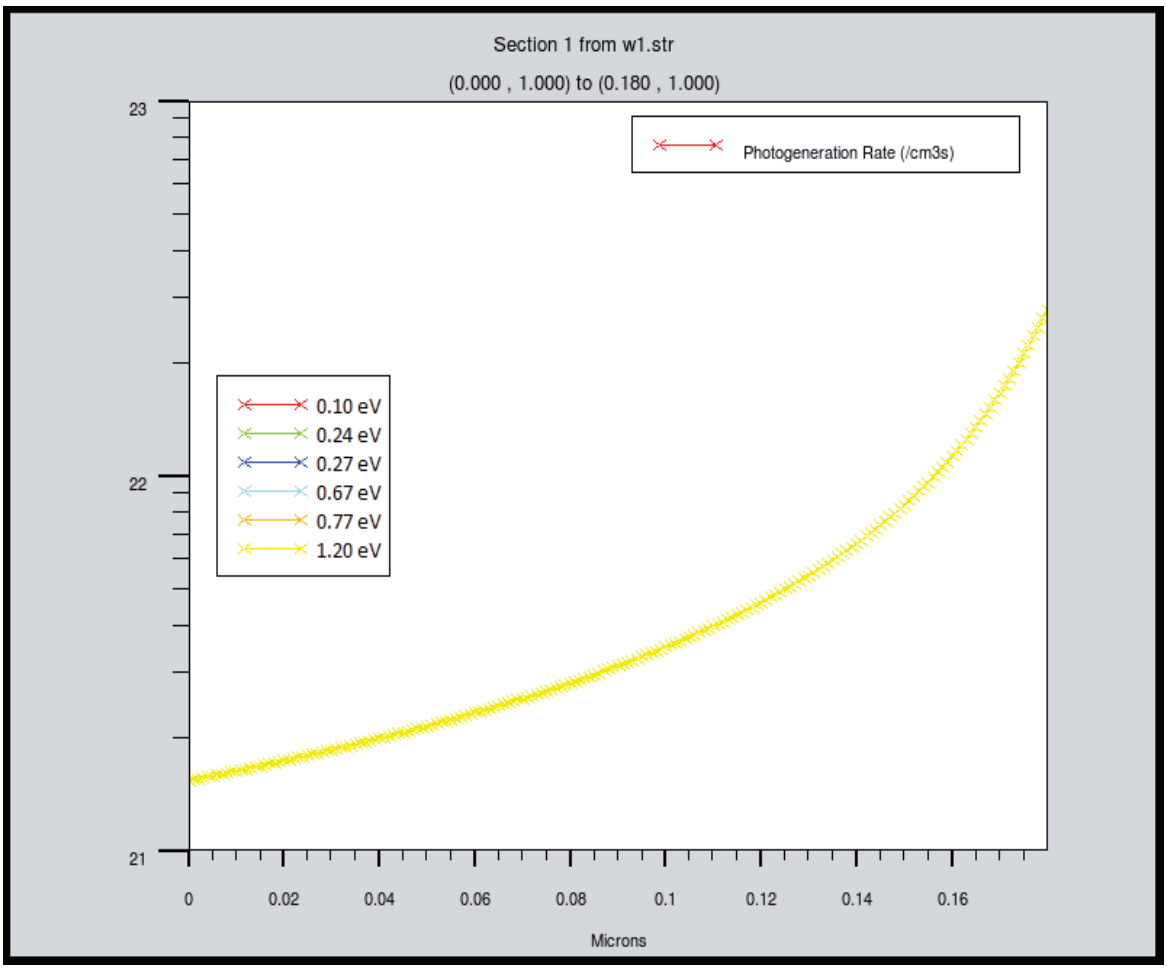

Photogeneration in radial direction at y=1 micron in device 4a-4f

Figure 2.39.

Comment:

Photogeneration in radial direction of the device is independent of the electrode material.

2.6.8. Potential Profile in the device:

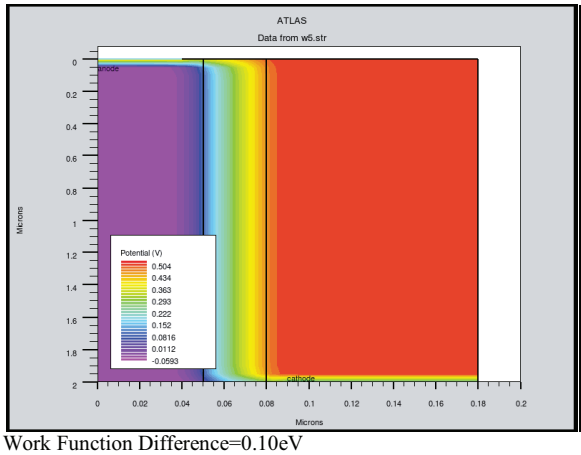

Work Function Difference=0.10eV

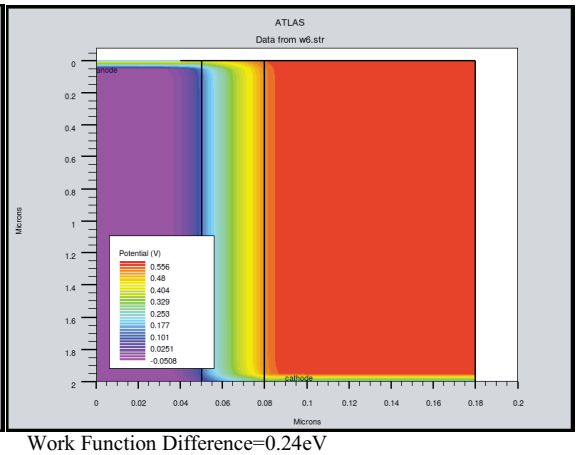

Work Function Difference=0.24eV

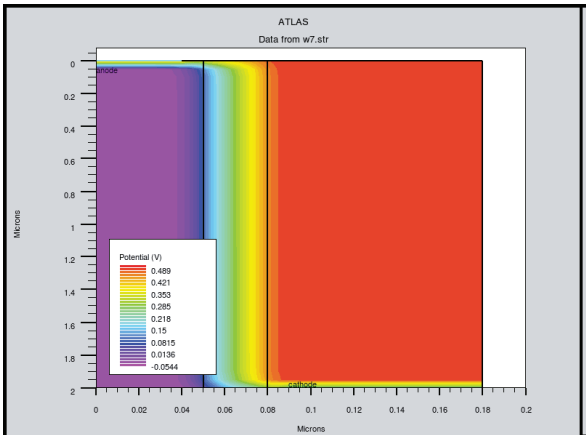

Work Function Difference=0.27eV

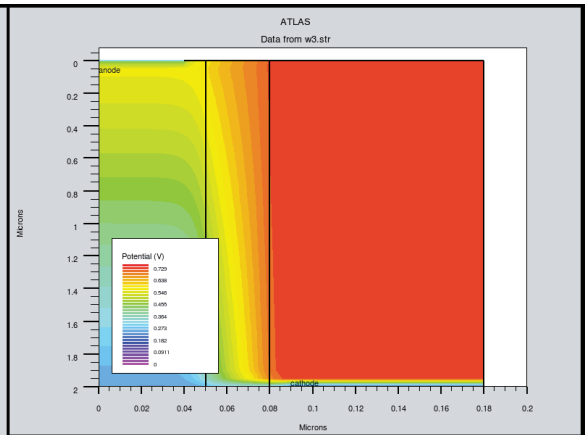

Work Function Difference=0.67eV

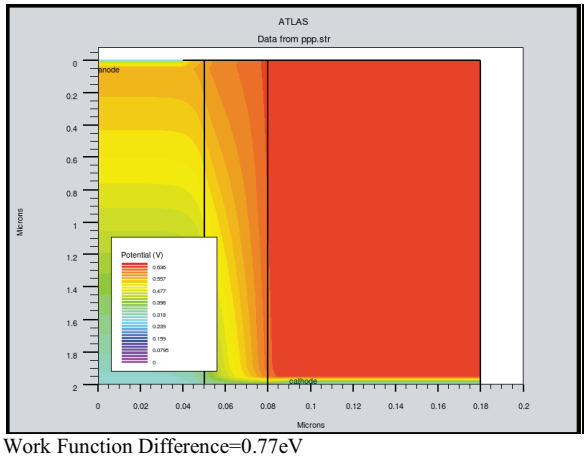

Work Function Difference=0.77eV

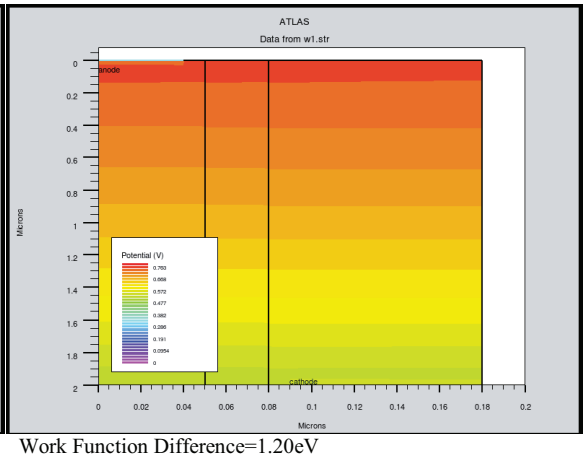

Work Function Difference=1.20eV

Potential profile of Device 4a-4f

Figure 2.40.

Comment:

It is observed that as the difference in the work function of the electrodes increases, the gradient of the potential profile becomes more vertical.

2.6.9. Other paramameters observed:

Cathode(eV)	4.53	4.53	4.53	4.63	4.53	4.1
Anode(eV)	4.63	4.77	4.8	5.3	5.3	5.3
Difference(eV)	0.1	0.24	0.27	0.67	0.77	1.2
Isc(A)	2.31E-10	2.32E-10	2.32E-10	2.32E-10	2.32E-10	2.44E-10
Voc(V)	0.0504559	0.184533	0.215151	0.272759	0.349962	0.601203
Pm(W)	4.03E-12	2.50E-11	3.09E-11	4.41E-11	6.49E-11	1.20E-10
Vm(V)	0.0299999	0.139998	0.16	0.2	0.3	0.5
Im(A)	1.34E-10	1.79E-10	1.93E-10	2.21E-10	2.16E-10	2.40E-10
FF(%)	34.6076	58.3115	61.8323	69.7262	79.8282	81.7804
Eff(%)	0.178157	1.10461	1.36593	1.95087	2.87003	5.30987
Vt(V)	0.183527	0.314888	0.343657	0.520155	0.639243	1.11109

Following Trends are observed with respect to the difference in work function of anode and cathode:

Impact of variation of electrode material on Short Circuit Current, Isc:

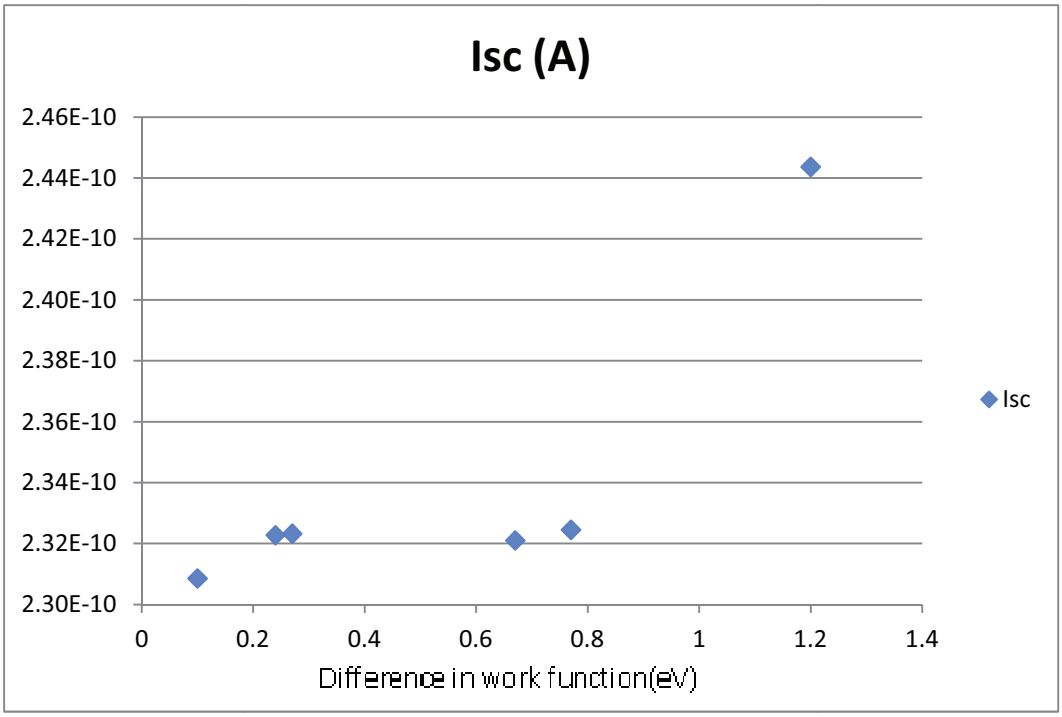

Impact of variation of electrode material on Isc
Figure 2.41.

Impact of variation of electrode material on Open Circuit Voltage, Voc:

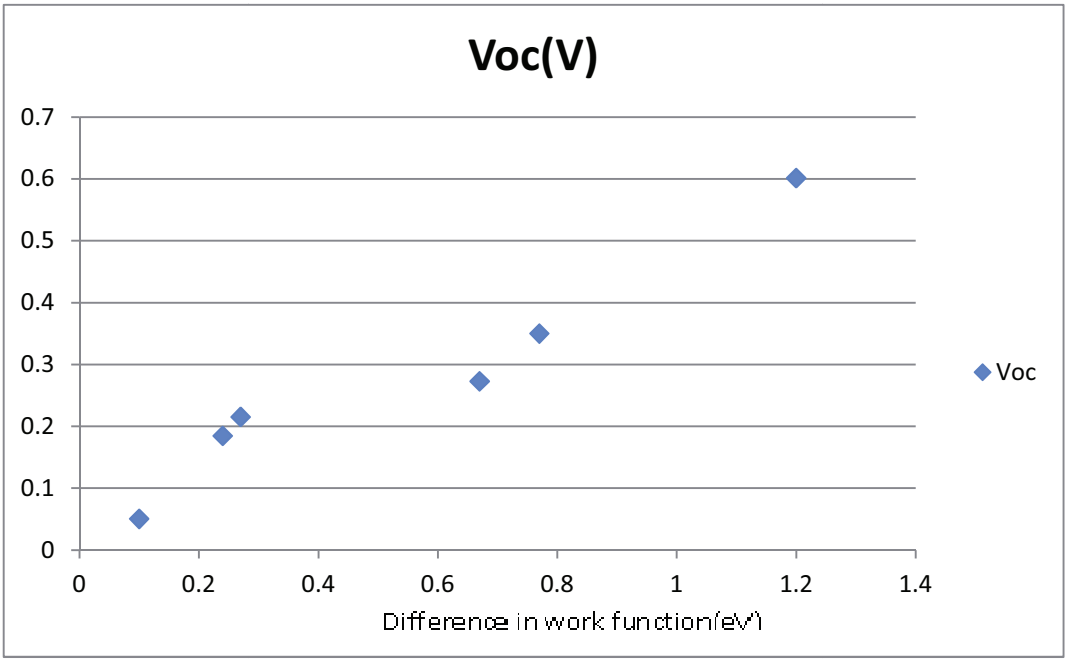

Impact of variation of electrode material on Voc
Figure 2.42.

Impact of variation of electrode material on Maximum Power Generated, Pm:

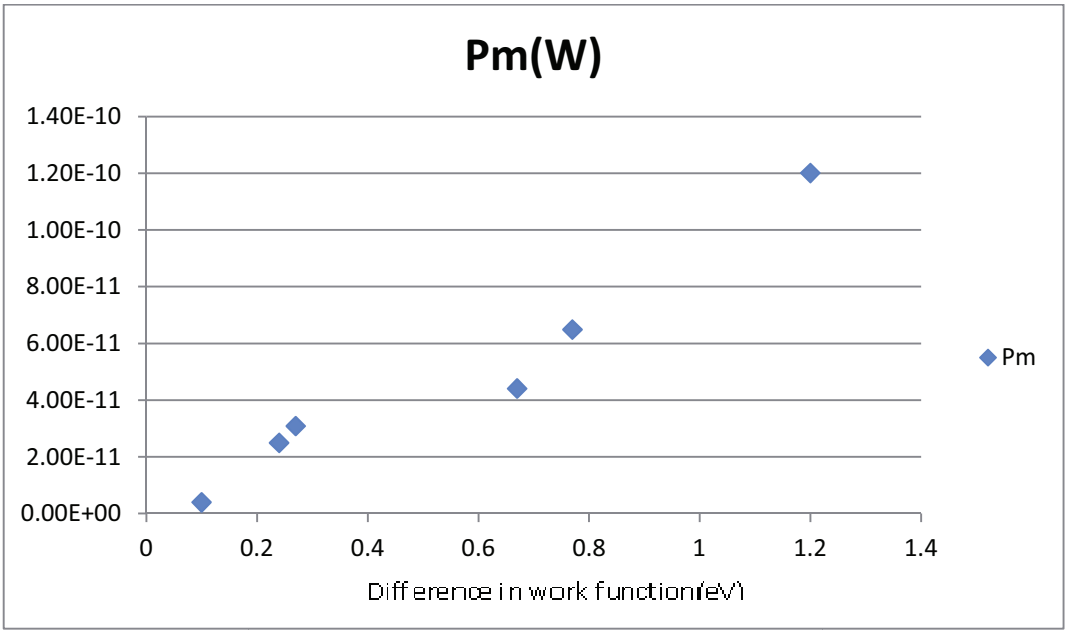

Impact of variation of electrode material on Pm
Figure 2.43.

Impact of variation of electrode material on Voltage at Maximum Power, Vm:

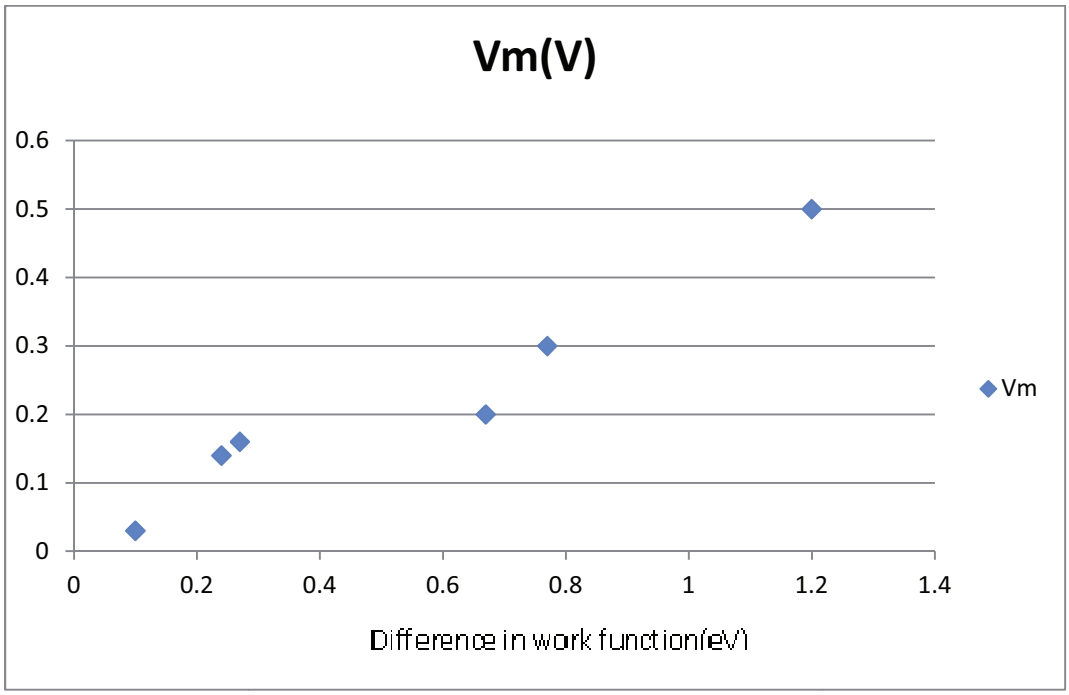

Impact of variation of electrode material on Vm

Figure 2.44.

Impact of variation of electrode material on Current at Maximum Power, Im:

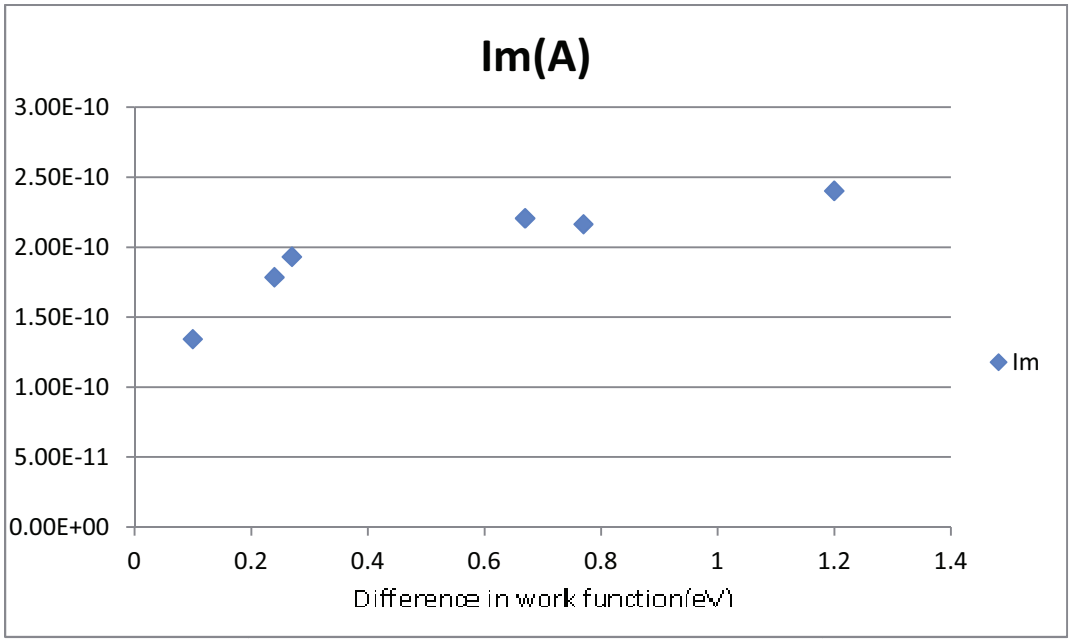

Impact of variation of electrode material on Im

Figure 2.45.

Impact of variation of electrode material on Fill Factor:

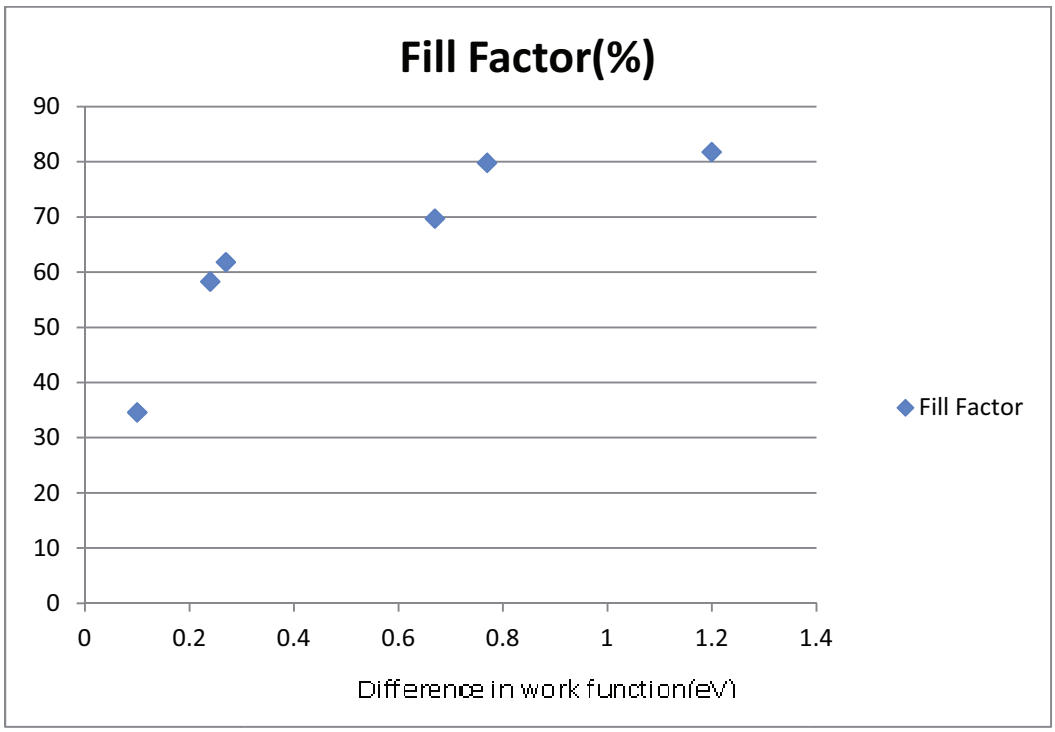

Impact of variation of electrode material on Fill Factor
Figure 2.46.

Impact of variation of electrode material on turn on voltage, Vt:

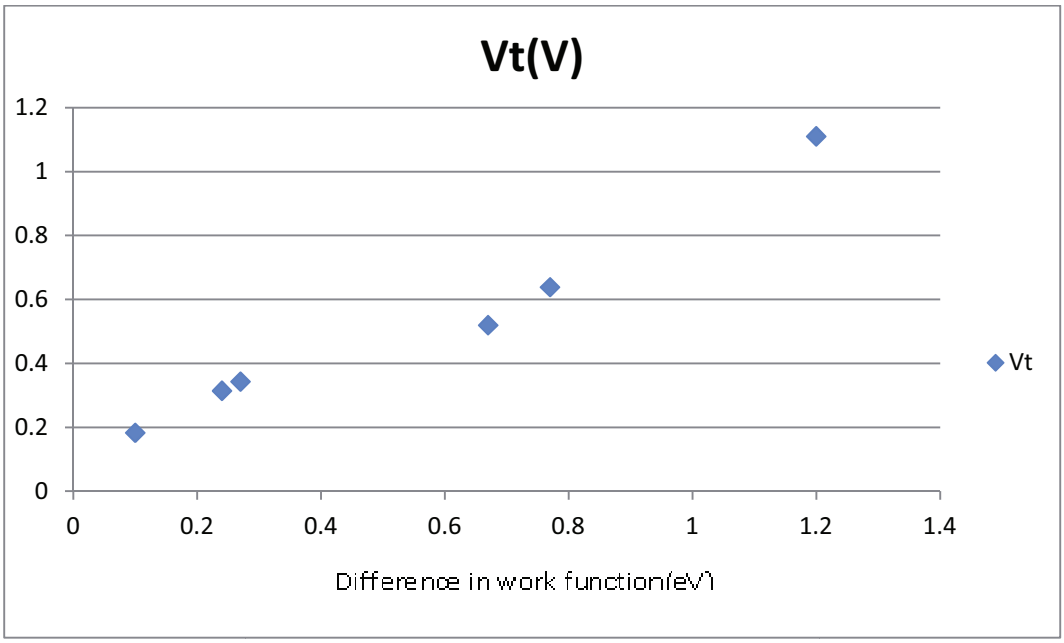

Impact of variation of electrode material on turn on voltage
Figure 2.47.

Impact of variation of electrode material on Efficiency, Eff:

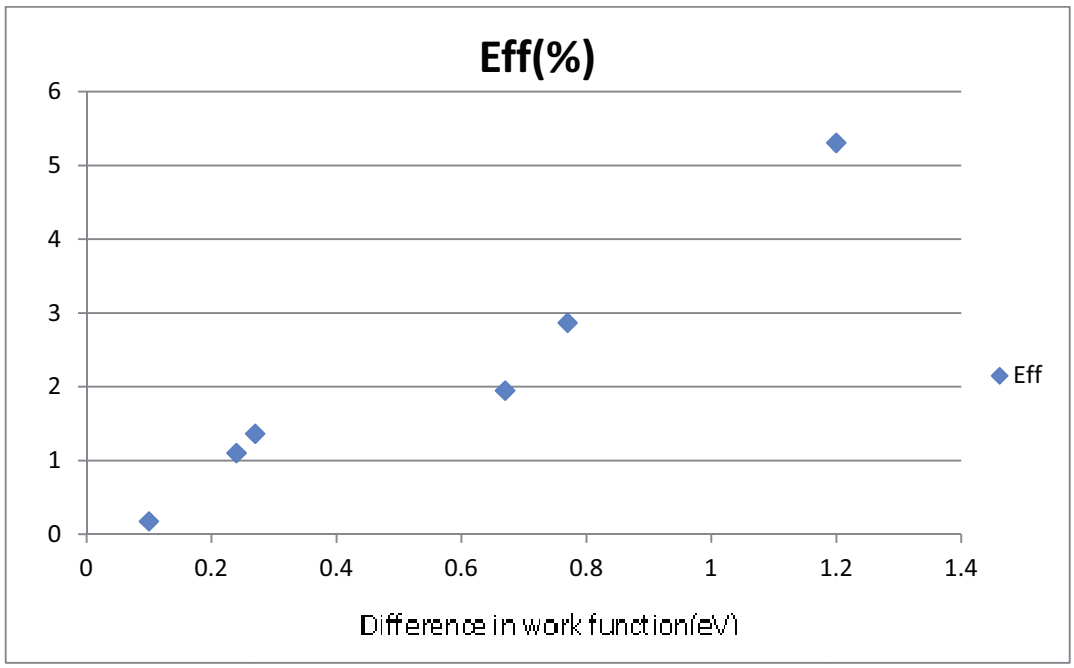

Impact of variation of electrode material on Efficiency
Figure 2.48.

2.6.10. Inference

On a general it is seen that with the increase in difference in work function of the electrodes, the parameters, Isc, Voc, Pm, Vm, Im, Fill Factor, Vt and Efficiency increases.

Taking a note of the fill factor, it can be said that as the difference in work function increases, fill factor increases, implying that the squareness of the i-v characteristic increases, thus approaching the ideal characteristic.

It is also inferred that device with electrodes with higher difference in workfunction is more efficient.

3. Conclusion

Due to the low efficiency of the silicon nanowire solar cell, they might not replace the conventional solar cell, but they definitely serve as a good option for on-chip integrated photovoltaic application.

It has been observed in this work that a coaxial silicon nanowire solar cell with p-i-n configuration made of polysilicon is superior than its counterpart in which the p-type core is made up of crystalline silicon. Thus making it possible to have a more efficient solar cell at lesser cost.

While keeping the total diameter of the solar cell constant and reducing the i-layer thickness, we get a more efficient solar cell at i-thickness equal to 28nm, than at i-thickness equal to 40nm.

Studying the variation in metal contacts of the solar cell, it has been observed that when the difference in the work function of electrodes is maximum, the i-v characteristic of the solar cell approaches the ideal characteristic with a high efficiency.

Thus it can be concluded that a silicon nanowire p-i-n solar cell made of polysilicon, with thin i-type layer(~28nm) and large difference in electrode work function serves as a high efficient solar cell with a characteristic approaching the ideal characteristic.

4. Limitations and Further Work

The main limitation of this thesis lies on the fact that, the simulation software, Silvaco Atlas version 5.16.3.R, doesn't support, photogeneration, while simulating device with quantum mechanics.

Thus while investigating i-layer thickness, the i-thickness was not reduced lower than 28nm, so that quantum confinement effect can be avoided.

Thus further work can be done by using a superior tool to study i-thickness lower than 28nm while taking into effect the quantum confinement effect.

The design studied in this thesis can be further modified and studied by making the following variations:

- Variation in doping Concentration
- Including an antireflective coating
- Keeping the geometry same and varying the material

5. References

[1] Solar cell, Wikipedia

[2] http://org.ntnu.no/solarcells/pages/generations.php

[3] Andrew D. Bates, "Novel optimization techniques for multijunction solar cell design using Silvaco ATLAS," M.S. thesis, Naval Postgraduate School, Monterey, CA, 2004.

[4] N. S. Lewis, Toward cost-effective solar energy use. Science 315, 798–801 (2007).

[5] N.S. Lewis & G. Crabtree, Basic Research Needs for Solar Energy Utilization.

[6] B. Tian, X. Zheng, T. J. Kempa, Y. Fang, N. Yu, G. Yu, J. Huang, and C. M. Lieber, "Coaxial silicon nanowires as solar cells and nanoelectronic power sources," Nature, vol. 449, no. 7164, pp. 885–889, Oct. 2007.

[7] Oka Kurniawan and Er Ping Li, Study of a Single Coaxial Silicon Nanowire for On-Chip Integrated Photovoltaic Application

[8] R. S. Friedman, M. C. McAlpine, D. S. Ricketts, D. Ham, and C. M. Lieber, Nanotechnology high-speed integrated nanowire circuits," Nature, vol. 434, no. 7037, p. 1085, Apr. 2005.

[9] W. U. Huynh, J. J. Dittmer, and A. P. Alivisatos, "Hybrid Nanorod-Polymer solar cells," Science, vol. 295, no. 5564, pp. 2425–2427, Mar. 2002

[10] J. B. Baxter and E. S. Aydil, "Nanowire-based dye-sensitized solar cells," Applied Physics Letters, vol. 86, no. 5, pp. 053 114–3, 2005.

[11] L. Tsakalakos, J. Balch, J. Fronheiser, M. Shih, S. F. LeBoeuf, M. Pietrzykowski, P. J. Codella, B. A. Korevaar, O. V. Sulima, J. Rand, A. Davuluru, and U. Rapol, "Strong broadband optical absorption in silicon nanowire films," Journal of Nanophotonics, vol. 1, no. 1, pp. 013 552–10, Jul. 2007.

[12] B.M. Kayes, H.A. Atwater & N.S.Lewis, Comparison of the device physics principles of planar and radial p-n junction nanorod solar cells. J. Appl. Phys. 97, 114302 (2005).

[13] Silvaco ATLAS user's manual, 2011.